Chronic ethanol exposure induces deleterious changes in cardiomyocytes derived from human induced pluripotent stem cells

Rui Liu[1,2], Fangxu Sun[3], Lawrence C. Armand[1], Ronghu Wu[3], and Chunhui Xu[1,4,*]

[1]Department of Pediatrics, Emory University School of Medicine and Children's Healthcare of Atlanta, Atlanta, GA 30322, USA

[2]Department of Pediatrics, The Third Xiangya Hospital of Central South University, Changsha, Hunan 410013, China

[3]School of Chemistry and Biochemistry and the Petit Institute for Bioengineering and Bioscience, Georgia Institute of Technology, Atlanta, GA 30332, USA

[4]Wallace H. Coulter Department of Biomedical Engineering, Georgia Institute of Technology and Emory University, Atlanta, GA 30322, USA

[*]Correspondence:

Chunhui Xu, PhD, Associate Professor, Department of Pediatrics, Emory University School of Medicine, 2015 Uppergate Drive, Atlanta, GA 30322. Email: chunhui.xu@emory.edu

Abstract

Chronic alcohol consumption in adults can induce cardiomyopathy, arrhythmias, and heart failure. In newborns, prenatal alcohol exposure can increase risk of congenital heart diseases. Understanding biological mechanisms involved in the long-term alcohol exposure-induced cardiotoxicity is pivotal to the discovery of therapeutic strategies. In this study, cardiomyocytes derived from human pluripotent stem cells (hiPSC-CMs) were treated with clinically relevant doses of ethanol for various durations up to 5 weeks. The treated cells were characterized for their cellular properties and functions, and global proteomic profiling was conducted to understand the molecular changes associated with long-term ethanol exposure. Increased cell death, oxidative stress, deranged Ca^{2+} handling, abnormal action potential, altered contractility, and suppressed structure development were observed in ethanol-treated cells. Many dysregulated proteins identified by global proteomic profiling were involved in apoptosis, heart contraction, and extracellular collagen matrix. In addition, several signaling pathways including the Wnt and TGFβ signaling pathways were affected due to long-term ethanol exposure. Therefore, chronic ethanol exposure to hiPSC-CMs induces cardiotoxicity, impairs cardiac functions, and alters protein expression and signaling pathways. This study demonstrates the utility of hiPSC-CMs as a novel model for chronic alcohol exposure study and provides the molecular mechanisms associated with long-term alcohol exposure to human cardiomyocytes.

Keywords

alcohol toxicity, cardiomyocyte, cardiotoxicity, disease modeling, induced pluripotent stem cell, proteomics

Introduction

Alcohol is the most consumed toxic and psychoactive substance with high potentials of physical and psychological addiction in human history [1]. It contributes to 3 million deaths per year globally and 5.1% of the global burden of disease [2]. As the second most affected body system by ethanol (EtOH), the cardiovascular system manifests varieties of alcohol-induced pathologies including atherosclerosis, hypertension, arrhythmias, and dilated cardiomyopathy [3]. Women are more susceptible to the damaging effects of EtOH than men at the same level of lifetime consumption [4-6]. Worse, according to Centers for Disease Control and Prevention, 4% of women overall had an alcohol use disorder in 2019 and 18% of childbearing-age women binge drink [7]. Maternal alcohol consumption increases the risk of fetal alcohol spectrum disorder (FASD). According to the National Institutes of Health-funded community studies, FASD prevalence in the United States is between 1 to 5 per 100 school children [8]. It is worth noting that congenital heart disease is a common clinical manifestation of FASD having a comorbid rate with FASD of 28.6% [9].

Understanding biological mechanisms involved in the alcohol-induced cardiotoxicity is pivotal to the discovery of preventive and therapeutic strategies. With respect to acute EtOH exposure-induced damage to cardiomyocyte (CM), studies have demonstrated the critical roles of oxidative stress, mitochondrial dysfunction, apoptosis, autophagy, and abnormal Ca^{2+} handling in various model systems including animal models [10, 11], murine and human primary CM models [12], and human induced pluripotent stem cell-derived CM (hiPSC-CM) model [13]. However, to date, most of the long-term and maternal EtOH exposure studies were conducted in animal models. Recently, several studies have uncovered the involvement of oxidative stress, autophagy, endoplasmic reticulum stress-mediated apoptosis, mitochondrial dysfunction, pro-inflammatory pathway activation, and cardiac contractile defects in the myocardium of mice and rats with long-term alcohol consumption [14-17]. Also, maternal EtOH exposure in neonatal mice, rats and zebrafishes could cause heart chamber defects, cardiac hypertrophy, fibrosis, apoptosis, oxidative stress, Ca^{2+} overload, and contractile dysfunction [18-21]. While animal models have provided significant insights into the mechanisms and phenotypes of chronic ethanol exposure,

physiological characteristics of the CM differ markedly in human and animals [22]. Hence, there is an unmet need to establish a human physiologically relevant model for the investigation of chronic EtOH exposure induced cardiotoxicity.

Human primary CMs are difficult to obtain in large quantities and preserve the contractile, electrophysiological and morphological properties for a long period *in vitro*, consequently impeding their application in chronic treatment studies [23]. In this context, hiPSCs have shown great potential to provide a limitless supply of physiologically relevant CMs owing to their regeneration and differentiation properties [24]. hiPSC-CMs have moderate expression of essential excitation-contraction coupling genes and functional sarcoplasmic reticulum and sarcomeres, which are key characteristics to CM function. hiPSC-CMs have been adopted broadly in cardiac disease modeling, including hypertrophic cardiomyopathy [25], dystrophy cardiomyopathy [26], and dilated cardiomyopathy [27]. hiPSC-CMs have also been used to study cardiotoxicity, including those induced by chemotherapeutic drug [28, 29], short-term EtOH exposure [13, 30], and iron overload [31].

Given the fetal characteristics of the hiPSC-CMs, these cells could be used as a cell model for studies of the prenatal alcohol exposure. Here, we report the findings from hiPSC-CMs subjected to long-term EtOH treatment−a novel model for the study of chronic alcohol exposure to human cardiac cells. We characterized long-term EtOH treatment-caused alterations of hiPSC-CMs at molecular, cellular, and functional levels, with a focus on cell survival, oxidative stress, Ca^{2+} handling, action potential (AP), contractility, structure development, and expression of the genes related to these processes. We also conducted global proteomic profiling of hiPSC-CMs treated with EtOH, which reveals the protein expression changes in cells after long-term EtOH exposure.

Materials and Methods

Sources of reagents

Vendor information and catalog numbers for major reagents are listed in Table S1.

Culture of hiPSCs and cardiomyocyte differentiation

hiPSC line IMR90 (WiCell Research Institute) was fed daily on Matrigel-coated plates with mTeSR1 medium, a defined medium for hiPSC culture. For CM differentiation, hiPSCs were induced using a growth factor-driven differentiation protocol [32, 33]. On the day of induction (day 0), medium was replaced with RPMI 1640 medium supplemented with 2% B27 minus insulin (a cell culture supplement) containing 100 ng/ml activin A. After induction for 24 h, the medium was replaced with fresh RPMI supplemented with 2% B27 minus insulin containing 10 ng/ml BMP4. From day 4 of differentiation, the medium was replaced with RPMI supplemented with 2% B27. On day 5, the cells were dissociated and reseeded into AggreWell400 plates to acquire cardiac spheres [34]. After 24 h, the cardiac spheres formed were collected and transferred to low-adhesion dishes for suspension culture. The medium was changed every other day. Cardiac spheres typically started beating spontaneously by day 7 to 9.

EtOH treatment

The EtOH-containing medium was freshly prepared by diluting pure ethyl alcohol in the culture medium to 2× test concentrations. Every three days, cardiac spheres were collected and resuspended in fresh culture medium, the same volume of 2× EtOH-working solutions were added in the dishes. Mineral oil was overlaid on top of the medium to prevent EtOH evaporation for both EtOH-treated and untreated groups [30]. Cardiac spheres were treated with EtOH at 0, 17, and 50 mM for up to 5 weeks. We had not examined if EtOH at these concentrations would affect osmotic pressure. However, since ethanol has a high plasma membrane permeability and can distribute rapidly throughout the cells [35], it is unlikely that low concentrations of ethanol as we used cause transmembrane difference in osmotic pressure.

Immunocytochemistry and cardiomyocyte purity assay

For immunocytochemistry, cardiac spheres were dissociated and reseeded into Matrigel-coated 96-well plates. Cells were fixed in 4% paraformaldehyde for 15 min and permeabilized using ice-cold methanol for

2 min at room temperature (RT). The cells were then incubated with 5% normal goat serum (NGS) in phosphate-buffered saline (PBS) at RT for 1 h then incubated with primary antibodies including α-actinin, NKX2-5, and cardiac troponin T (Table S2) in 3% NGS overnight at 4℃. After washing, the cells were incubated with the corresponding secondary antibodies at RT for 1 h in dark followed by counterstaining the nuclei with 7 μM Hoechst33342. Imaging was performed using an inverted microscope (ZEISS, Axio Vert.A1). For CM purity quantification, images were acquired and quantitatively analyzed using ArrayScan XTI Live High Content Platform (Thermo Fisher Scientific). The percentages of cells positive for NKX2-5 and α-actinin were calculated as CM purity [29].

Live/dead staining

For live/dead cellular imaging, cardiac spheres were collected and incubated with 1 μM ethidium homodimer-1 and 0.25 μM calcein-AM working solution in culture medium in the dark at 37˚C for 20 min. Images were acquired using an inverted microscope (ZEISS, Axio Vert.A1).

Flow cytometry

For the flow cytometry experiment, cardiac spheres were dissociated, and the single cell suspensions were adjusted to 1×10^6 cells/ml in PBS. For live/dead cell quantification, 5×10^5 cells/sample were stained with Live/Dead Fixable Near-IR Dead Cell Stain Kit according to the manufacturer's instructions. After washing with PBS, cells were fixed in 4% paraformaldehyde for 15 min. Cells were then washed and resuspended in 1% BSA in PBS solution and analyzed by Cytoflex Flow Cytometer (Beckman Coulter). For apoptosis quantification, 1×10^5 cells/sample were prepared and stained using PE Annexin V Apoptosis Detection Kit following the manufacturer's instructions. Cells were analyzed within 1 h by Guava easyCyte Flow Cytometer (MilliporeSigma).

RNA extraction and quantitative real-time polymerase chain reaction (qRT-PCR)

Aurum total RNA mini kit was used to extract RNA and SuperScript VILO cDNA Synthesis Kit was used to reversely transcribe 1μg of RNA into cDNA per the manufacturer's instructions. qRT-PCR was performed on Applied Biosystems 7500 real-time PCR systems (Thermo Fisher Scientific) using the iTaq SyBr green master mix. Human specific PCR primers (Table S3) for the genes examined were retrieved from open access websites (https://pga.mgh.harvard.edu/primerbank/). All samples were normalized to the level of the housekeeping gene *GAPDH*. Relative expression levels were calculated by the 2^-ΔΔCt method.

Detection of reactive oxygen species (ROS)

For the detection of intracellular and mitochondrial ROS, cardiac spheres were dissociated and reseeded into Matrigel-coated 96-well plates. The cells were incubated with 12.5 μM carboxy-H_2DCFDA or 1 μM MitoSOX Red, and 7 μM Hoechst working solutions in warm 0.25% bovine serum albumin (BSA) in PBS solution for 15 min at 37ºC in dark. Images were acquired and analyzed using ArrayScan XTI Live High-Content Platform [13]. Signal detection of H_2DCFDA and MitoSOX Red was restriced to the cytoplasm with a mask that extended 7 units from the nucleus. Mean fluorescence intensities of H_2DCFDA and MitoSOX Red of cells were quantified and used as readout.

Ca^{2+} kinetics imaging

For intracellular Ca^{2+} transient analysis, cardiac spheres were dissociated and replated into Matrigel-coated 96-well plates at a low density for single-cell distribution. The cells were then incubated with 5μM cell-permeant dye Fluo-4 AM working solution in 1× normal Tyrode solution (148 mM NaCl, 4 mM KCl, 0.5 mM $MgCl_2 \cdot 6H_2O$, 0.3 mM $NaPH_2O_4 \cdot H_2O$, 5 mM HEPES, 10 mM D-Glucose, 1.8 mM $CaCl_2 \cdot H_2O$, pH adjusted to 7.4 with NaOH) for 20 min at 37ºC in dark. Fluorescence images were recorded and analyzed using the ImageXpress Micro XLS System (Molecular Devices) at a frequency of 5 Hz for 12 s [29].

Membrane potential dynamics imaging

For live cell membrane potential analysis, cardiac spheres were dissociated and replated onto Matrigel-coated cover glasses at a low density as single-cell distribution and incubated with the working solution of voltage-sensitive dye FluoVolt (diluted according to the instruction in the FluoVolt Membrane Potential Kit) in 1× normal Tyrode solution for 20 min at RT in dark. Recordings of membrane potential fluorescence were acquired at 40x magnification in line-scan mode using an inverted laser confocal scanning microscope (Olympus FV1000) equipped with FluoView software (Olympus). The cover glasses with cells were placed in a microscope chamber and continuously perfused at 37°C with 1× normal Tyrode solution [36]. The recordings were analyzed with Clampfit 10.6 software (Molecular Devices).

Video-based analysis of contractility

Cardiac spheres were dissociated and replated into Matrigel-coated 96-well plates at a density of 4-5×10^4 cells/well. The cells were then cultured to form a sheet of spontaneous beating cells in each well. Beating was recorded using a phase-contrast inverted microscope (ZEISS, Axio Vert.A1) for 15 s/well. Video-based analysis of contractility parameters was performed with Matlab (R2019a) algorithm by motion tracking function [37].

Proteomic analysis

For protein extraction, cardiac spheres were collected and resuspended in the lysis buffer (50 mM HEPES pH =7.4, 150 mM NaCl, 0.5% SDC, 10 units/mL benzonase, and 1 tablet/10 mL protease inhibitor) at 4°C for 45 min. The protein concentration was determined using the BCA assay, and the amounts of proteins in all six samples were then normalized based on their concentrations. Proteins were reduced with 5 mM DTT (56°C, 30 min), followed by alkylation with 14 mM iodoacetamide (IAA) at RT for 30 min in the dark, and then were purified through the methanol-chloroform protein precipitation method. The isolated proteins were digested with trypsin in a buffer containing 50 mM HEPES (pH 8.5), 1.6 M urea at 37°C overnight. After digestion, peptides were purified using tC18 Sep-Pak cartridges. Tandem mass tag (TMT) labeling and fractionation, LC-MS/MS analysis, database search, data filtering, peptide quantification, and

bioinformatic analysis were conducted as described previously [30]. Proteins were considered being up- or down-regulated when the abundance changed by >1.2-fold between two groups. Gene functional enrichment was performed with Metascape [38]. Gene Ontology (GO) terms with P <0.05 were considered significantly enriched by differentially expressed proteins (DEPs).

Statistical methods

Data were analyzed and graphed in Excel, GraphPad Prism 8, FlowJo, and RStudio. Data are presented as mean ± SD. Comparisons were conducted via one-way ANOVA test followed by multiple comparison procedures (Dunnett method) or two-sided Chi-square test with significant differences defined by P <0.05 (*), P <0.01 (**), P <0.001 (***), P <0.0001 (****). Sample sizes were given for each experiment.

Results

Chronic EtOH exposure decreases hiPSC-CM viability

We first generated cardiac spheres containing enriched hiPSC-CMs (Fig. 1) and then from differentiation day 14 treated them with EtOH at 0, 17, and 50 mM for up to 5 weeks. We note that 17 mM EtOH concentration is the legal limit in the United States to drive (blood alcohol concentration of 0.08%) and 50 mM corresponds to the dose associated with the excitement stage of alcohol intoxication in clinic [39]. Additionally, 17 and 50 mM were used in other studies of EtOH exposure in hiPSC-CMs, human primary CMs, and murine CMs [12, 13].

To assess the cell viability upon EtOH exposure, we stained cardiac spheres following 1, 3, and 5-week exposure to ethanol using ethidium homodimer-1 (for dead cells) and calcein (for live cells) (Fig. 2a). We quantified the degree of cell death caused by 5-week EtOH exposure by flow cytometric analysis. Compared with the non-treatment group, the 17 mM EtOH treatment cultures contained 5% less live cells (Near-IR negative cells) and 50 mM EtOH treatment cultures contained 10% less live cells (Fig. 2b). We also quantified cell viability by trypan blue staining after the 5-week EtOH exposure. Compared with the

non-treatment group, the 17 mM EtOH treatment cultures contained 13% less of live cells and 50 mM EtOH treatment cultures contained 20% less of live cells (Fig. 2c).

To evaluate if the cell death in EtOH-treated hiPSC-CMs was associated with apoptosis, we performed flow cytometric analysis of the EtOH-treated cells stained with Annexin V and 7-Aminoactinomycin D (7-AAD). The number of cells in the early stage of apoptosis (positive for Annexin V+ and negative for 7-AAD) significantly increased upon 50 mM EtOH exposure, and the number of cells in the late stage of apoptosis (positive for Annexin V and 7-AAD) were similar among cells treated with 0, 17 and 50 mM EtOH (Fig. 2d). We also examined the expression of apoptosis-related genes by qRT-PCR in cells exposed to EtOH for 5 weeks. The detected levels of the genes *BAX, TP53, CDKN1A,* and *PLK1* were remarkably lower in hiPSC-CMs treated with 50 mM EtOH compared with non-treatment group; three of them (*BAX, CDKN1A,* and *PLK1*) were also decreased in 17 mM EtOH-treated cells (Fig. 2e).

Taken together, these results indicate that chronic EtOH treatment reduced the viability of hiPSC-CMs via apoptosis.

Chronic EtOH treatment causes oxidative stress in hiPSC-CMs

To examine if the cell death in long-term EtOH-treated hiPSC-CMs was associated with increased cellular oxidative stress, we measured intracellular ROS by H_2DCFDA probe and mitochondrial ROS by MitoSOX probe in cells treated with EtOH for 1, 3, and 5 weeks. Increased ROS signals were detected in the cells treated with EtOH (Fig. 3a). The relative level of intracellular oxidative stress was 41% higher in cells treated with 17 mM EtOH and 60% higher in cells treated with 50 mM EtOH than in untreated cells. The relative level of mitochondrial oxidative stress was 20% higher in cells treated with 17 mM EtOH and 46% higher in cells treated with 50 mM EtOH than in untreated cells (Fig. 3b).

We next examined the expression of oxidative stress-related genes by qRT-PCR in cardiac spheres exposed to EtOH for 5 weeks. The expression of two superoxide dismutase family of genes (*SOD1* and *SOD3*), a reductase encoding gene (*PRDX5*), two glutathione related genes (*GSR*, *GPX1*), and an NADPH oxidase encoding gene (*NOX4*) was significantly reduced in cells treated with 50 mM EtOH compared with

non-treatment group (Fig. 3c and Fig. S1). Of note, *SOD3* level detected was 45% lower in cells exposed to 17 mM EtOH compared with non-treatment group and even lower (66%) in cells treated with 50 mM EtOH. The expression of other oxidative stress-related genes, including *SOD2*, *NQO2*, *NOX1*, *NOX5*, *DUOX1*, and *DUOX2,* did not show significant change (Fig. S2).

Chronic EtOH treatment damages cardiac function in hiPSC-CMs

Regular contraction of the heart is an event that requires effective electric activation, coordinated movement of Ca^{2+}, and functional contractile apparatus at the CM level. To investigate the effect of long-term EtOH exposure on CM function, first we assessed intracellular Ca^{2+} transients in cells treated with EtOH for 5 weeks. As shown by the representative traces (Fig. 4a), 6 types of whole cell Ca^{2+} release events were observed. Specifically, type i (mostly consistent amplitudes and rhythmicity, typical cardiac Ca^{2+} transient morphology, and no obvious spontaneous Ca^{2+} release between transients) was categorized as normal cells and type ii-vi were categorized as abnormal cells (ii and iii, significant inconsistent amplitudes or intervals; iv and v, oscillation occurrence; vi, unrecognizable single transient morphology). Using this classification, we counted the numbers of cells exhibiting normal or abnormal Ca^{2+} transients and calculated the proportion of each category for each culture condition (Fig. 4b). In the non-treatment group, the majority of the cells exhibited normal Ca^{2+} transients, but the percentage of cells exhibiting abnormal Ca^{2+} transients increased to 51% for 17 mM EtOH treatment group and 53% for 50 mM EtOH treatment group. Three types of abnormal Ca^{2+} transients were observed in the non-treatment group (type ii 1%, type iv 28%, type v 4%). Four types of abnormal Ca^{2+} transients were observed in the EtOH treatment groups (17 mM EtOH treatment group: type iii 2%, type iv 31%, type vi 14%, type vi 4%; 50 mM EtOH treatment group: type ii 7%, type iv 25%, type vi 17%, type vi 4%).

Next, we evaluated the action potential (AP) of EtOH-treated hiPSC-CMs. In one evaluation, we counted the numbers and calculated the proportion of cells exhibiting normal or abnormal AP in each treatment group. Cells with normal AP had rapid depolarization and smoothly descending repolarization kinetics and cells with abnormal AP exhibited afterdepolarizations (Fig. 4c). The proportion of the cells

exhibiting normal AP was 97% in the non-treatment group, 87% in the group treated with 17 mM EtOH and 79% in the group treated with 50 mM EtOH (Fig. 4d). In another evaluation, we analyzed AP parameters of the cells (Fig. 4e, 4f, and S3). APD100 (duration of depolarization plus repolarization) and decay time (duration of depolarization) were significantly increased by 16% and 32% in 17 mM EtOH-treated cells; 19% and 38% in 50 mM EtOH-treated cells. Rise time (duration of depolarization), APD50 (duration of depolarization plus repolarization to 50% of amplitude), and half amplitude decay time (duration of repolarization to 50% of amplitude) were markedly decreased by 20%, 34%, and 43%, respectively, in 17 mM EtOH-treated cells, 19%, 40%, and 47%, respectively, in 50 mM EtOH-treated cells.

We also quantified the expression of genes encoding the components of Ca^{2+}, K^+, and Na^+ channels (which are crucial to Ca^{2+} transient and AP) by qRT-PCR in hiPSC-CMs (Fig. 4g). The expression of the Ca^{2+} channel protein-encoding gene *ATP2A2* was decreased in cells treated with 17 mM EtOH and the expression of the K^+ channel protein encoding gene *KCNA4* and the Na^+ channel protein encoding gene *SCN5A* was reduced in cells treated with 17 and 50 mM EtOH compared with non-treatment group.

To identify the effect of long-term EtOH exposure on CM contractility, we recorded spontaneous beating and quantified beating indexes of the hiPSC-CMs. The velocities of contraction and relaxation of each CM beating were recorded for 15 s (Fig. 5a). Treatment of hiPSC-CMs with EtOH at 17 and 50 mM markedly decreased the beating rate and maximum relaxation without distinct maximum contraction alteration compared with non-treatment group (Fig. 5b). Specifically, the beating rates decreased to 23 and 24 beats/min in cells exposed to 17 and 50 mM EtOH, respectively, from the 45 beats/min in untreated cells. The maximum relaxation in cells exposed to 17 mM EtOH was reduced by 14%, which further dropped by 15% more in cells exposed to 50 mM EtOH. In addition, the expression of several genes encoding contractile fiber parts was lower in EtOH-treated cells than in untreated cells as detected by qRT-PCR, including *TNNT2*, *TTN*, *ACTN1*, and the light chain of myosin encoding genes *MYL2* and *MYL7* (Fig. 5c). Taken together, these results show that chronic EtOH exposure of hiPSC-CMs resulted in intracellular Ca^{2+} handling dysfunction, altered membrane potential, and impaired CM contractility.

Chronic EtOH treatment suppresses cardiac structure development in hiPSC-CMs

To examine the effect of long-term EtOH exposure on CM sarcomeric organization, we conducted immunostaining of α-actinin, a marker for myofibrillar Z-discs, in cells treated with EtOH for 5 weeks. We evaluated the cells for their overall appearance of myofibrillar structure and categorized them into 3 levels of sarcomeric development as described previously [34, 40]: Score 1 cells are α-actinin-positive but without clear sarcomeric striations; Score 2 cells have diffused point staining pattern and striations in partial cell area; and Score 3 cells have organized, definitive myofibrillar structure with clear paralleled bands of z-discs distributed throughout the cell area (Fig. 6a). Compared with the non-treatment group, EtOH-treated CMs had fewer cells with clear sarcomeric striations (Fig. 6b). In addition, the expression of α-actinin decreased in EtOH-treated hiPSC-CMs (Fig. 6c). Based on the CM size and shape, the cell spread area decreased in EtOH-treated hiPSC-CMs, whereas the cell width/length ratio was similar. These observations demonstrate that chronic EtOH exposure suppressed hiPSC-CM structure development.

Chronic EtOH treatment of hiPSC-CMs alters the expression of proteins identified by proteomic analysis

To further evaluate the molecular alteration induced by long-term EtOH exposure, we collected cell lysates from the duplicates of cardiac spheres that had been treated with or without EtOH for 5 weeks and quantitated proteins. The correlation of the protein levels among the duplicates were high (Fig. 7a), suggesting high reproducibility between replicates. The analysis revealed that 453 proteins in the 17 mM EtOH treatment group were significantly different from the untreated group (upregulated: 400, downregulated: 53) and 251 proteins in the 50 mM EtOH treatment were significantly different from the untreated group (upregulated: 213, downregulated: 38) (Fig. 7b). Among these differentially expressed proteins (DEPs), 151 were upregulated and 16 were downregulated in both of the 17 and 50 mM EtOH treatment groups (Fig. 7b). As shown in Table S4, among the top 15 upregulated proteins in cells with the EtOH treatment, 4 were collagen trimer components (COL3A1, COL11A1, FCN3, and COL1A1). And

among the top 15 downregulated proteins by EtOH treatment, 7 were correlated to muscle contraction (CRYAB, MYH1, CASQ1, TNNI3, CSRP3, ACTA1, and SLMAP).

To determine the biological processes affected by EtOH treatment, we performed GO analysis among the up- and downregulated proteins in the 17 and 50 mM EtOH treatment groups, respectively. In the 17 mM EtOH treatment group, the upregulated proteins were associated with the extracellular matrix (ECM) organization (48 proteins), supramolecular fiber organization (61 proteins), actin cytoskeleton organization (56 proteins), response to wounding (53 proteins), and cell-substrate adhesion (34 proteins). The downregulated proteins were associated with the muscle system process (11 proteins), cellular amino acid metabolic process (8 proteins), heart contraction (7 proteins), heart development (8 proteins), and energy derivation by oxidation of organic compounds (6 proteins). In the 50 mM EtOH treated group, the upregulated proteins were related to the ECM organization (22 proteins), supramolecular fiber organization (27 proteins), response to wounding (25 proteins), collagen fibril organization (9 proteins), and regulation of cell adhesion (23 proteins). The downregulated proteins were associated with the muscle system process (9 proteins), actomyosin structure organization (6 proteins), negative regulation of organelle organization (4 proteins), cellular nitrogen compound catabolic process (4 proteins), and cellular Ca^{2+} homeostasis (3 proteins) (Fig. 7c).

In addition, we performed GO analysis among the overlapping DEPs between 17 and 50 mM EtOH treatment groups. Fig. 7d and Fig. S4 include the detailed information about the interested GO terms linked with specific DEPs. In this analysis, individual proteins could be linked with more than one GO term. For example, secreted frizzled related protein 1 (SFRP1) is involved in ECM, regulation of mitogen-activated protein kinase (MAPK) cascade, response to transforming growth factor β (TGFβ), bone morphogenetic protein (BMP) signaling pathway, Wingless/Int (Wnt) signaling pathway, and apoptotic signaling pathway; collagen type I α1 (COL1A1) is known to be involved in ECM, collagen trimer, response to oxidative stress, response to TGFβ, and Wnt signaling pathway. Also, elastin microfibril interfacer 1 (EMILIN1) is known to contribute to ECM, collagen trimer, response to TGFβ, and regulation of MAPK cascade; and BCL2

interacting protein 3 (BNIP3) and tumor necrosis factor receptor associated protein 1 (TRAP1) are involved in response to oxidative stress and apoptotic signaling pathway.

Discussion

Long-term treatment with EtOH causes severe detrimental effects on hiPSC-CMs as indicated by cell death, excessive reactive oxygen species, deranged Ca^{2+} handling, abnormal AP, dysfunctional contractility, and suppressed structure development. By performing the proteomic and bioinformatic analysis, we have identified proteins and pathways affected by chronic EtOH treatment, which aids in deciphering the underlying molecular mechanisms comprehensively. These observations were obtained from 3D cell culture with enriched hiPSC-CMs. Compared with two-dimensional cell culture, 3D culture displays more metabolic maturation features [41] and can better mimic the cellular microenvironment *in vivo*, consequently attaining higher fidelity to capture cell responses to drugs [42-44].

Among the detrimental effects of long-term EtOH, CM functional measurements showed higher rates of arrhythmogenic Ca^{2+} release events and afterdepolarizations of AP in EtOH-treated hiPSC-CMs. We also observed shortening of APD50 while prolongation of APD100 in hiPSC-CMs exposed to EtOH. Both of the AP duration abnormalities are known to contribute to severe arrythmias including atrial fibrillation, ventricular tachyarrhythmias and torsades des pointes [45-47]. Cardiac Ca^{2+} handling and membrane voltage regulation are bidirectionally coupled. Specifically, spontaneous Ca^{2+} release during diastole can trigger afterdepolarizations and elongate AP duration; conversely, afterdepolarizations can promote spontaneous Ca^{2+} waves [48]. Na^+ and K^+ also play pivotal roles in regulating AP since depolarization is mainly triggered by Na^+ current and repolarization is mostly determined by K^+ current. Because these metal cations are tightly controlled by corresponding ion channels, the alterations of these specific channels at the gene and protein levels would result in aforementioned electrophysiological defects [49]. Indeed, we found decreased expression levels of genes encoding metal ion channels, such as ATPase sarcoplasmic/endoplasmic reticulum Ca^{2+} transporting 2 (*ATP2A2*), potassium voltage-gated channel subfamily A member 4 (*KCNA4*), and sodium voltage-gated channel alpha subunit 5 (*SCN5A*) in EtOH-

treated hiPSC-CMs. Hence, chronic EtOH exposure may target multiple subcellular sites resulting in complex phenotypes of cardiac Ca^{2+} handling and AP defects, which was also observed in acute EtOH exposure-induced cardiac arrhythmogenic effects [50]. These cardiac defects could result from chronic EtOH-induced oxidative stress; particularly for CMs, ROS can modify ion channels, which may trigger Ca^{2+} handling and AP abnormalities, and ultimately result in arrythmias and dysfunctional contraction [51].

To exert effective contraction and relaxation of CMs, a highly organized contractile apparatus represented by myofibrils is also required. Sarcomeres as structural and functional units of myofibrils are composed of thin filaments (formed by actin, troponin, and tropomyosin), thick filaments (formed by myosin), Z-disks (formed by α-actinin), and titin [52]. In this study, we observed lower level of sarcomeric striations, dysregulated expression of α-actinin, troponin and myosin at the gene and protein levels, and decreased expression of titin in EtOH-treated CMs. Since EtOH treatment suppressed cardiac structure development and the expression of structural proteins, it is possible that impaired CM maturation could contribute to the changes in gene expression mediated by EtOH. The observed structural changes are consistent with the changes in contractility parameters of the cells exposed to EtOH. Interestingly, relaxation force reduction without contraction force decrease is a frequent symptom observed in chronic alcoholics [53].

Similar to acute EtOH exposure-induced cardiotoxicity in hiPSC-CM model [13] and rat models [11, 54], we found that oxidative stress also played a role in chronic EtOH exposure-induced deleterious effects on hiPSC-CMs, as indicated by elevated mitochondrial and intracellular ROS levels. We also detected markedly decreased expression of genes encoding glutathione-related enzymatic antioxidants, which could contribute to chronic EtOH exposure-induced oxidative stress in hiPSC-CMs. ROS is known to directly interact with cellular components including lipids, proteins and DNA, affect the structure and function of important intracellular molecules, and culminate in cell dysfunction and even cell death [55]. Indeed, we observed higher rates of apoptotic and dead cells in hiPSC-CMs exposed to EtOH. Furthermore, consistent with these observations, we also detected increased expression of several pro-apoptosis genes and decreased expression levels of several anti-apoptosis genes in EtOH-treated cells, including cyclin-

dependent kinase inhibitor 1A (*CDKN1A*), polo-like kinase 1 (*PLK1*), BNIP3, cholecystokinin (CCK), and protein disulfide isomerase family A member 3 (PDIA3). However, increased expression of TRAP1 (an anti-apoptosis protein) and decreased expression of SFRP1 and *BAX* (pro-apoptosis protein/gene) were also observed in hiPSC-CMs exposed to EtOH. These observations suggest that distinct pro- and anti-apoptosis genes are involved in both oxidative stress-induced cell death as well as adaptive survival of the cells to long-term EtOH exposure. In other studies, ROS can induce myocardial apoptosis through the activation of both the extrinsic and intrinsic apoptosis initiation signaling pathways or inhibition of the protective mechanisms of the cell [56].

The cardiac ECM is an intricate architectural network surrounding and interconnecting CMs. It is composed mainly of fibrillar collagen, creating strength and plasticity [57]. In the heart, the major fibrillar collagens are collagen types I and III, which are responsible for maintaining alignment of myofibrils via collagen-integrin-cytoskeleton-myofibril connections in CMs [58]. In this study, proteomic profiling identified significantly upregulated expression of extracellular collagen matrix related proteins in EtOH-treated hiPSC-CMs. For example, in comparison with non-treatment group, cells exposed to 17 mM EtOH expressed 93% more of COL1A1, 87% more of collagen type XI α1 (COL11A1), and 85% more of collagen type III α1 (COL3A1). Accumulation of collagen has been correlated with cardiac fibrosis, hypertrophy cardiomyopathy, and diastolic and systolic dysfunction [59]. In view of the remarkable changes of collagen matrix proteins in EtOH-treated hiPSC-CMs, these proteins could be potential biomarkers for alcoholic cardiomyopathy diagnosis. Indeed, growing evidence demonstrated that COL1A1 could serve as a biomarker candidate in a variety of cardiac diseases, such as diabetic cardiomyopathy and heart failure [60, 61].

Several signal transduction pathways, such as TGFβ and Wnt signaling, have been linked to the pathophysiology of inappropriate ECM production. Activation of TGFβ signaling pathway can promote a wide range of cardiac pathophysiology processes, including CM apoptosis, hypertrophic responses, inflammation, and ECM deposition [62]. Wnt signaling is an important pathway in normal development and disease states of the heart, and increased expression of Wnt proteins occurs during cardiac hypertrophy

[63]. Recent studies also demonstrate that the crosstalk between these two pathways is crucial to the development of cardiac hypertrophy [64]. In this study, TGFβ and Wnt signaling pathways were highly enriched from the DEPs in EtOH-treated cells. For instance, compared with non-treatment group, 17 mM EtOH-treated cells expressed 55% more of TGFβ2, 49% more of periostin (a TGFβ responsive promoter [65]), 43% more of frizzled class receptor 7 (FZD7, a Wnt protein receptor [63]), and 45% more of Wnt2. We also note that SFRP5, an inhibitor of Wnt signaling, was also significantly upregulated in EtOH-treated cells. This result suggests a possible role of SFRP5 in adaptive survival of EtOH-treated cells, as SFRP5 has cardioprotective potential in cardiac diseases [66], which implies that inhibition of Wnt signaling pathway could be a therapeutic target for chronic EtOH exposure-induced cardiac hypertrophy. In addition, TGFβ can also activate other pathways including phosphoinositide-3 kinase (PI3K) signaling and MAPK cascades to result in cardiac hypertrophy [67]. Indeed, we observed that EtOH treatment caused upregulation of proteins involved in these two pathways as identified by proteomics.

Our results show that chronic EtOH exposure caused cytotoxicity and affected cellular functions in a dose-dependent manner. In addition, the toxicity doses of chronic EtOH exposure observed in this study are lower than those of acute EtOH in the same cell line observed in our previous study [13]. The dose response could be affected by the genetic background of the cell lines used. For example, cell lines derived from individuals with faster rates of alcohol metabolism may be less sensitive to EtOH toxicity than those derived from individuals with slower rates of alcohol metabolism. Additional experiments with various genetic background could provide further insights into chronic EtOH toxicity. In addition, further experimentation on the leads from global proteomic profiling can provide clarification on which of these pathways/processes are important in mediating chronic EtOH toxicity. For example, one could modulate selected pathways by overexpression or knockdown of key genes and examine if the toxicity of chronic EtOH toxicity is affected.

In conclusion, our study has demonstrated chronic EtOH treatment of hiPSC-CMs induces apoptosis and cell death, oxidative stress, abnormal Ca^{2+} handling, AP, contractility, and structure development. Consistent with the cell-level assessments, many dysregulated proteins identified by global

proteomic profiling are involved in apoptosis, oxidative stress, heart contraction, and intra- and extracellular structures. Furthermore, our study also implicated the alteration of several signaling pathways, including the Wnt and TGFβ signaling pathways, in chronic EtOH exposure-induced cardiotoxicity.

Supplemental Information

Supplemental Information includes Table S1-S4 and Fig. S1-S4.

Declarations

The authors have no disclosures to report and declare no competing financial interests.

Funding

This study was supported by the National Institutes of Health [R21AA025723, R01HL136345, and R01AA028527]; NSF-CASIS (National Science Foundation-Center for the Advancement of Science in Space) [CBET 1926387]; the Center for Pediatric Technology at Emory University; and Georgia Institute of Technology; and Imagine, Innovate and Impact (I3) Funds from the Emory School of Medicine and through the Georgia CTSA NIH award [UL1-TR002378].

Availability of data and material

The raw files of proteomics have been deposited in the public MassIVE database with the identifier MSV000087349.

Authors' contributions

R.L., F.S., R.W., and C.X. designed experiments. R.L. and F.S. performed experiments. R.L., F.S., and L.C.A. analyzed data. R.L., F.S., L.C.A., R.W., and C.X. wrote the manuscript. All authors contributed to the discussion of results and editing and final approval of the manuscript.

Acknowledgements

We thank Changfa Shu, Dr. Yuhong Du and Dr. Haian Fu at Emory Chemical Biology Discovery Center and the Department of Pharmacology and Chemical Biology, Emory University School of Medicine for their support on the ImageXpress Micro XLS System and Guava easyCyte Flow Cytometer.

References

1. Degenhardt, L., Chiu, W. T., Sampson, N., Kessler, R. C., Anthony, J. C., Angermeyer, M., Bruffaerts, R., de Girolamo, G., Gureje, O., Huang, Y., et al. (2008) Toward a global view of alcohol, tobacco, cannabis, and cocaine use: Findings from the WHO world mental health surveys. *PLoS Med*, *5*(7), e141.
2. World Health Organization. Global status report on alcohol and health. Available at: https://apps.who.int/iris/bitstream/handle/10665/274603/9789241565639-eng.pdf?ua=1 [Accessed Feb 27, 2021].
3. Fernandez-Sola, J. (2020) The effects of ethanol on the heart: Alcoholic cardiomyopathy. *Nutrients*, *12*(2), 572.
4. Erol, A. & Karpyak, V. M. (2015) Sex and gender-related differences in alcohol use and its consequences: Contemporary knowledge and future research considerations. *Drug Alcohol Depend*, *156*, 1-13.
5. Mogos, M. F., Salemi, J. L., Phillips, S. A., & Piano, M. R. (2019) Contemporary appraisal of sex differences in prevalence, correlates, and outcomes of alcoholic cardiomyopathy. *Alcohol Alcohol*, *54*(4), 386-395.
6. Urbano-Marquez, A., Estruch, R., Fernandez-Sola, J., Nicolas, J. M., Pare, J. C., & Rubin, E. (1995) The greater risk of alcoholic cardiomyopathy and myopathy in women compared with men. *JAMA*, *274*(2), 149-154.

7. Centers for Disease Control and Prevention. Excessive alcohol use is a risk to women's health. Available at: https://www.cdc.gov/alcohol/fact-sheets/womens-health.htm [Accessed Feb 27, 2021].

8. Centers for Disease Control and Prevention. Fetal alcohol spectrum disorders. Available at: https://www.cdc.gov/ncbddd/fasd/data.html [Accessed Mar 1, 2021].

9. Burd, L., Deal, E., Rios, R., Adickes, E., Wynne, J., & Klug, M. G. (2007) Congenital heart defects and fetal alcohol spectrum disorders. *Congenit Heart Dis*, *2*(4), 250-255.

10. El-Mas, M. M. & Abdel-Rahman, A. A. (2014) Nongenomic effects of estrogen mediate the dose-related myocardial oxidative stress and dysfunction caused by acute ethanol in female rats. *Am J Physiol Endocrinol Metab*, *306*(7), E740-747.

11. Zhu, Z., Huang, Y., Lv, L., Tao, Y., Shao, M., Zhao, C., Xue, M., Sun, J., Niu, C., Wang, Y., et al. (2018) Acute ethanol exposure-induced autophagy-mediated cardiac injury via activation of the ROS-JNK-Bcl-2 pathway. *J Cell Physiol*, *233*(2), 924-935.

12. Mustroph, J., Wagemann, O., Lebek, S., Tarnowski, D., Ackermann, J., Drzymalski, M., Pabel, S., Schmid, C., Wagner, S., Sossalla, S., et al. (2018) SR Ca(2+)-leak and disordered excitation-contraction coupling as the basis for arrhythmogenic and negative inotropic effects of acute ethanol exposure. *J Mol Cell Cardiol*, *116*, 81-90.

13. Rampoldi, A., Singh, M., Wu, Q., Duan, M., Jha, R., Maxwell, J. T., Bradner, J. M., Zhang, X., Saraf, A., Miller, G. W., et al. (2019) Cardiac toxicity from ethanol exposure in human-induced pluripotent stem cell-derived cardiomyocytes. *Toxicol Sci*, *169*(1), 280-292.

14. Mouton, A. J., El Hajj, E. C., Ninh, V. K., Siggins, R. W., & Gardner, J. D. (2020) Inflammatory cardiac fibroblast phenotype underlies chronic alcohol-induced cardiac atrophy and dysfunction. *Life Sci*, *245*, 117330.

15. Yang, M., Wang, S., Fu, S., Wu, N. N., Xu, X., Sun, S., Zhang, Y., & Ren, J. (2021) Deletion of the E3 ubiquitin ligase, Parkin, exacerbates chronic alcohol intake-induced cardiomyopathy through an Ambra1-dependent mechanism. *Br J Pharmacol*, *178*(4), 964-982.

16. Nakashima, M. A., Silva, C. B. P., Gonzaga, N. A., Simplicio, J. A., Omoto, A. C. M., Tirapelli, L. F., Tanus-Santos, J. E., & Tirapelli, C. R. (2019) Chronic ethanol consumption increases reactive oxygen species generation and the synthesis of pro-inflammatory proteins in the heart through TNFR1-dependent mechanisms. *Cytokine*, *121*, 154734.

17. Wang, W., Liu, T., Liu, Y., Yu, L., Yan, X., Weng, W., Lu, X., & Zhang, C. (2021) Astaxanthin attenuates alcoholic cardiomyopathy via inhibition of endoplasmic reticulum stress-mediated cardiac apoptosis. *Toxicol Appl Pharmacol*, *412*, 115378.

18. Ninh, V. K., El Hajj, E. C., Ronis, M. J., & Gardner, J. D. (2019) N-acetylcysteine prevents the decreases in cardiac collagen I/III ratio and systolic function in neonatal mice with prenatal alcohol exposure. *Toxicol Lett*, *315*, 87-95.

19. Nguyen, V. B., Probyn, M. E., Campbell, F., Yin, K. V., Samuel, C. S., Zimanyi, M. A., Bertram, J. F., Black, M. J., & Moritz, K. M. (2014) Low-dose maternal alcohol consumption: Effects in the hearts of offspring in early life and adulthood. *Physiol Rep*, *2*(7), e12087.

20. Ren, J., Wold, L. E., Natavio, M., Ren, B. H., Hannigan, J. H., & Brown, R. A. (2002) Influence of prenatal alcohol exposure on myocardial contractile function in adult rat hearts: Role of intracellular calcium and apoptosis. *Alcohol Alcohol*, *37*(1), 30-37.

21. Sarmah, S. & Marrs, J. A. (2017) Embryonic ethanol exposure affects early- and late-added cardiac precursors and produces long-lasting heart chamber defects in zebrafish. *Toxics*, *5*(4), 35.

22. Guo, G. R., Chen, L., Rao, M., Chen, K., Song, J. P., & Hu, S. S. (2018) A modified method for isolation of human cardiomyocytes to model cardiac diseases. *J Transl Med*, *16*(1), 288.

23. Mitcheson, J. S., Hancox, J. C., & Levi, A. J. (1998) Cultured adult cardiac myocytes: Future applications, culture methods, morphological and electrophysiological properties. *Cardiovasc Res*, *39*(2), 280-300.

24. Hnatiuk, A. P., Briganti, F., Staudt, D. W., & Mercola, M. (2021) Human iPSC modeling of heart disease for drug development. *Cell Chem Biol*, *28*(3), 271-282.

25. Knight, W. E., Cao, Y., Lin, Y. H., Chi, C., Bai, B., Sparagna, G. C., Zhao, Y., Du, Y., Londono, P., Reisz, J. A., et al. (2021) Maturation of pluripotent stem cell-derived cardiomyocytes enables modeling of human hypertrophic cardiomyopathy. *Stem Cell Reports*, *16*(3), 519-533.

26. Kamdar, F., Das, S., Gong, W., Klaassen Kamdar, A., Meyers, T. A., Shah, P., Ervasti, J. M., Townsend, D., Kamp, T. J., Wu, J. C., et al. (2020) Stem cell-derived cardiomyocytes and beta-adrenergic receptor blockade in Duchenne muscular dystrophy cardiomyopathy. *J Am Coll Cardiol*, *75*(10), 1159-1174.

27. McDermott-Roe, C., Lv, W., Maximova, T., Wada, S., Bukowy, J., Marquez, M., Lai, S., Shehu, A., Benjamin, I., Geurts, A., et al. (2019) Investigation of a dilated cardiomyopathy-associated variant in BAG3 using genome-edited iPSC-derived cardiomyocytes. *JCI Insight*, *4*(22), e128799.

28. Kitani, T., Ong, S. G., Lam, C. K., Rhee, J. W., Zhang, J. Z., Oikonomopoulos, A., Ma, N., Tian, L., Lee, J., Telli, M. L., et al. (2019) Human induced pluripotent stem cell model of trastuzumab-induced cardiac dysfunction in breast cancer patients. *Circulation*, *139*(21), 2451-2465.

29. Liu, R., Li, D., Sun, F., Rampoldi, A., Maxwell, J. T., Wu, R., Fischbach, P., Castellino, S. M., Du, Y., Fu, H., et al. (2020) Melphalan induces cardiotoxicity through oxidative stress in cardiomyocytes derived from human induced pluripotent stem cells. *Stem Cell Res Ther*, *11*(1), 470.

30. Liu, R., Sun, F., Forghani, P., Armand, L. C., Rampoldi, A., Li, D., Wu, R., & Xu, C. (2020) Proteomic profiling reveals roles of stress response, Ca(2+) transient dysregulation, and novel signaling pathways in alcohol-induced cardiotoxicity. *Alcohol Clin Exp Res*, *44*(11), 2187-2199.

31. Rhee, J. W., Yi, H., Thomas, D., Lam, C. K., Belbachir, N., Tian, L., Qin, X., Malisa, J., Lau, E., Paik, D. T., et al. (2020) Modeling secondary iron overload cardiomyopathy with human induced pluripotent stem cell-derived cardiomyocytes. *Cell Rep*, *32*(2), 107886.

32. Jha, R., Xu, R. H., & Xu, C. (2015) Efficient differentiation of cardiomyocytes from human pluripotent stem cells with growth factors. *Methods Mol Biol*, *1299*, 115-131.

33. Laflamme, M. A., Chen, K. Y., Naumova, A. V., Muskheli, V., Fugate, J. A., Dupras, S. K., Reinecke, H., Xu, C., Hassanipour, M., Police, S., et al. (2007) Cardiomyocytes derived from human embryonic stem cells in pro-survival factors enhance function of infarcted rat hearts. *Nat Biotechnol*, *25*(9), 1015-1024.

34. Jha, R., Wu, Q., Singh, M., Preininger, M. K., Han, P., Ding, G., Cho, H. C., Jo, H., Maher, K. O., Wagner, M. B., et al. (2016) Simulated microgravity and 3D culture enhance induction, viability, proliferation and differentiation of cardiac progenitors from human pluripotent stem cells. *Sci Rep*, *6*, 30956.

35. Brahm, J. (1983) Permeability of human red cells to a homologous series of aliphatic alcohols. Limitations of the continuous flow-tube method. *J Gen Physiol*, *81*(2), 283-304.

36. Gentillon, C., Li, D., Duan, M., Yu, W. M., Preininger, M. K., Jha, R., Rampoldi, A., Saraf, A., Gibson, G. C., Qu, C. K., et al. (2019) Targeting HIF-1alpha in combination with PPARalpha activation and postnatal factors promotes the metabolic maturation of human induced pluripotent stem cell-derived cardiomyocytes. *J Mol Cell Cardiol*, *132*, 120-135.

37. Huebsch, N., Loskill, P., Mandegar, M. A., Marks, N. C., Sheehan, A. S., Ma, Z., Mathur, A., Nguyen, T. N., Yoo, J. C., Judge, L. M., et al. (2015) Automated video-based analysis of contractility and calcium flux in human-induced pluripotent stem cell-derived cardiomyocytes cultured over different spatial scales. *Tissue Eng Part C Methods*, *21*(5), 467-479.

38. Zhou, Y., Zhou, B., Pache, L., Chang, M., Khodabakhshi, A. H., Tanaseichuk, O., Benner, C., & Chanda, S. K. (2019) Metascape provides a biologist-oriented resource for the analysis of systems-level datasets. *Nat Commun*, *10*(1), 1523.

39. Intoximeters. Alcohol and the human body. Available at: https://www.intox.com/physiology/ [Accessed Feb 27, 2021].

40. Han, J., Wu, Q., Xia, Y., Wagner, M. B., & Xu, C. (2016) Cell alignment induced by anisotropic electrospun fibrous scaffolds alone has limited effect on cardiomyocyte maturation. *Stem Cell Res*, *16*(3), 740-750.

41. Correia, C., Koshkin, A., Duarte, P., Hu, D., Carido, M., Sebastiao, M. J., Gomes-Alves, P., Elliott, D. A., Domian, I. J., Teixeira, A. P., et al. (2018) 3D aggregate culture improves metabolic maturation of human pluripotent stem cell derived cardiomyocytes. *Biotechnol Bioeng*, *115*(3), 630-644.

42. Fiedler, L. R., Chapman, K., Xie, M., Maifoshie, E., Jenkins, M., Golforoush, P. A., Bellahcene, M., Noseda, M., Faust, D., Jarvis, A., et al. (2019) MAP4K4 inhibition promotes survival of human stem cell-derived cardiomyocytes and reduces infarct size in vivo. *Cell Stem Cell*, *24*(4), 579-591 e512.

43. Langhans, S. A. (2018) Three-dimensional in vitro cell culture models in drug discovery and drug repositioning. *Front Pharmacol*, *9*, 6.

44. Duval, K., Grover, H., Han, L. H., Mou, Y., Pegoraro, A. F., Fredberg, J., & Chen, Z. (2017) Modeling physiological events in 2D vs. 3D cell culture. *Physiology (Bethesda)*, *32*(4), 266-277.

45. Park, S. J., Zhang, D., Qi, Y., Li, Y., Lee, K. Y., Bezzerides, V. J., Yang, P., Xia, S., Kim, S. L., Liu, X., et al. (2019) Insights into the pathogenesis of catecholaminergic polymorphic ventricular tachycardia from engineered human heart tissue. *Circulation*, *140*(5), 390-404.

46. Ellermann, C., Mittelstedt, A., Wolfes, J., Willy, K., Leitz, P., Reinke, F., Eckardt, L., & Frommeyer, G. (2020) Action potential triangulation explains acute proarrhythmic effect of aliskiren in a whole-heart model of atrial fibrillation. *Cardiovasc Toxicol*, *20*(1), 49-57.

47. Lan, H., Xu, Q., El-Battrawy, I., Zhong, R., Li, X., Lang, S., Cyganek, L., Borggrefe, M., Zhou, X., & Akin, I. (2020) Ionic mechanisms of disopyramide prolonging action potential duration in human-induced pluripotent stem cell-derived cardiomyocytes from a patient with short QT syndrome type 1. *Front Pharmacol*, *11*, 554422.

48. Song, Z., Ko, C. Y., Nivala, M., Weiss, J. N., & Qu, Z. (2015) Calcium-voltage coupling in the genesis of early and delayed afterdepolarizations in cardiac myocytes. *Biophys J*, *108*(8), 1908-1921.

49. Landstrom, A. P., Dobrev, D., & Wehrens, X. H. T. (2017) Calcium signaling and cardiac arrhythmias. *Circ Res*, *120*(12), 1969-1993.

50. Sutanto, H., Cluitmans, M. J. M., Dobrev, D., Volders, P. G. A., Bebarova, M., & Heijman, J. (2020) Acute effects of alcohol on cardiac electrophysiology and arrhythmogenesis: Insights from multiscale in silico analyses. *J Mol Cell Cardiol*, *146*, 69-83.

51. Tse, G., Yan, B. P., Chan, Y. W., Tian, X. Y., & Huang, Y. (2016) Reactive oxygen species, endoplasmic reticulum stress and mitochondrial dysfunction: The link with cardiac arrhythmogenesis. *Front Physiol*, *7*, 313.

52. Gautel, M. & Djinovic-Carugo, K. (2016) The sarcomeric cytoskeleton: From molecules to motion. *J Exp Biol*, *219*(Pt 2), 135-145.

53. Fernandez-Sola, J., Nicolas, J. M., Pare, J. C., Sacanella, E., Fatjo, F., Cofan, M., & Estruch, R. (2000) Diastolic function impairment in alcoholics. *Alcohol Clin Exp Res*, *24*(12), 1830-1835.

54. Guan, Z., Lui, C. Y., Morkin, E., & Bahl, J. J. (2004) Oxidative stress and apoptosis in cardiomyocyte induced by high-dose alcohol. *J Cardiovasc Pharmacol*, *44*(6), 696-702.

55. Schieber, M. & Chandel, N. S. (2014) ROS function in redox signaling and oxidative stress. *Curr Biol*, *24*(10), R453-462.

56. Xu, T., Ding, W., Ji, X., Ao, X., Liu, Y., Yu, W., & Wang, J. (2019) Oxidative stress in cell death and cardiovascular diseases. *Oxid Med Cell Longev*, *2019*, 9030563.

57. Rienks, M., Papageorgiou, A. P., Frangogiannis, N. G., & Heymans, S. (2014) Myocardial extracellular matrix: An ever-changing and diverse entity. *Circ Res*, *114*(5), 872-888.

58. Bildyug, N. (2019) Extracellular matrix in regulation of contractile system in cardiomyocytes. *Int J Mol Sci*, *20*(20), 5054.

59. Bi, X., Song, Y., Song, Y., Yuan, J., Cui, J., Zhao, S., & Qiao, S. (2021) Collagen cross-linking is associated with cardiac remodeling in hypertrophic obstructive cardiomyopathy. *J Am Heart Assoc*, *10*(1), e017752.

60. Johnson, R., Nxele, X., Cour, M., Sangweni, N., Jooste, T., Hadebe, N., Samodien, E., Benjeddou, M., Mazino, M., Louw, J., et al. (2020) Identification of potential biomarkers for predicting the early onset of diabetic cardiomyopathy in a mouse model. *Sci Rep*, *10*(1), 12352.

61. Hua, X., Wang, Y. Y., Jia, P., Xiong, Q., Hu, Y., Chang, Y., Lai, S., Xu, Y., Zhao, Z., & Song, J. (2020) Multi-level transcriptome sequencing identifies COL1A1 as a candidate marker in human heart failure progression. *BMC Med*, *18*(1), 2.

62. Liu, G., Ma, C., Yang, H., & Zhang, P. Y. (2017) Transforming growth factor beta and its role in heart disease. *Exp Ther Med*, *13*(5), 2123-2128.

63. Dawson, K., Aflaki, M., & Nattel, S. (2013) Role of the Wnt-Frizzled system in cardiac pathophysiology: A rapidly developing, poorly understood area with enormous potential. *J Physiol*, *591*(6), 1409-1432.

64. Yousefi, F., Shabaninejad, Z., Vakili, S., Derakhshan, M., Movahedpour, A., Dabiri, H., Ghasemi, Y., Mahjoubin-Tehran, M., Nikoozadeh, A., Savardashtaki, A., et al. (2020) TGF-beta and WNT signaling pathways in cardiac fibrosis: Non-coding RNAs come into focus. *Cell Commun Signal*, *18*(1), 87.

65. Landry, N. M., Cohen, S., & Dixon, I. M. C. (2018) Periostin in cardiovascular disease and development: A tale of two distinct roles. *Basic Res Cardiol*, *113*(1), 1.

66. Gross, J. C. & Zelarayan, L. C. (2018) The mingle-mangle of Wnt signaling and extracellular vesicles: Functional implications for heart research. *Front Cardiovasc Med*, *5*, 10.

67. Hanna, A. & Frangogiannis, N. G. (2019) The role of the TGF-beta superfamily in myocardial infarction. *Front Cardiovasc Med*, *6*, 140.

Figure Legends

Fig. 1 Experimental scheme of hiPSC differentiation and hiPSC-CM generation. **(a)** Overall experiment design. **(b)** Representative images of immunocytochemistry revealing the majority of the cells in culture

were positive for cardiac transcription factor NKX2-5, and structural proteins cardiac troponin T and α-actinin at day 12. **(c)** Representative images acquired from ArrayScan and quantification of NKX2-5- or α-actinin-positive cell percentages indicated enrichment of CMs in the cultures at day 12.

Fig. 2 Chronic EtOH exposure decreases hiPSC-CM viability. **(a)** Representative images of live (calcein, green fluorescence) and dead (ethidium homodimer-1, red fluorescence) cells in hiPSC-CM culture treated with EtOH for 1, 3, and 5 weeks. **(b)** Representative dot plots and quantification of live cells by flow cytometric analysis. hiPSC-CMs were treated with EtOH for 5 weeks and analyzed by Live/Dead Near-IR Dead Cell Stain Kit (n =5 cultures). The cells gated in the rectangle box are Near-IR negative cells (live cells), and the rest are dead cells. **(c)** Quantification of viable cell numbers in hiPSC-CMs treated with EtOH for 5 weeks using trypan blue staining and hemocytometer cell counting (n =3 cultures). The initial cell numbers of each group were the same before treatment. **(d)** Representative dot plots and quantification of apoptotic cells by flow cytometric analysis of hiPSC-CMs treated with EtOH for 5 weeks using PE Annexin V Apoptosis Detection Kit (n =3 cultures). The upper right part of the dot plots indicates cells positive for both Annexin V and 7-AAD; the lower right part indicates cells positive for Annexin V only. **(e)** qRT-PCR analysis showing relative mRNA levels of apoptosis-related genes including *BCL2*, *BAX*, *TP53*, *CDKN1A*, and *PLK1* in hiPSC-CMs treated with EtOH for 5 weeks (n =3 cultures). Relative cell number and mRNA level were calculated based on the average values of EtOH-treated group vs. untreated group. Comparisons were conducted between each treatment group and non-treatment group via one-way ANOVA test. *, *P* value <0.05; **, *P* value <0.01; ***, *P* value <0.001; ****, *P* value <0.0001.

Fig. 3 Chronic EtOH treatment causes oxidative stress in hiPSC-CMs. **(a)** Representative images of intracellular (DCFDA, green fluorescence) and mitochondrial (MitoSOX, red fluorescence) ROS production in hiPSC-CMs treated with EtOH for 5 weeks. **(b)** Quantification of intracellular and mitochondrial ROS production in hiPSC-CMs treated with EtOH for 1, 3, and 5 weeks (n =4 cultures). **(c)** qRT-PCR analysis showing relative mRNA levels of oxidative stress-related genes in hiPSC-CMs treated

with EtOH for 5 weeks (n =3 cultures). Relative MFI and mRNA levels were calculated based on the average values of EtOH-treated group vs. untreated group. Comparisons were conducted between each treatment group and non-treatment group via one-way ANOVA test. *, *P* value <0.05; **, *P* value <0.01; ***, *P* value <0.001; ****, *P* value <0.0001.

Fig. 4 Chronic EtOH treatment damages Ca^{2+} handling and AP in hiPSC-CMs. **(a)** Illustrative traces presenting different types of intracellular Ca^{2+} transients in hiPSC-CMs. Type i: normal Ca^{2+} transients; Types ii to vi: abnormal Ca^{2+} transients. **(b)** Stacked bar chart showing proportions of hiPSC-CMs exhibiting each type of Ca^{2+} transients following the treatment with EtOH for 5 weeks. Sample sizes (n) were denoted at the top of each bar. **(c)** Illustrative traces presenting normal and abnormal AP dynamics in hiPSC-CMs. **(d)** Stacked bar chart showing proportions of hiPSC-CMs exhibiting normal and abnormal AP following the treatment with EtOH for 5 weeks. Sample sizes (n) were denoted at the top of each bar. **(e, f)** Quantification of AP amplitude and duration changes (n =28 cells for 0 and 50 mM EtOH treatment groups, n =40 cells for 17 mM EtOH treatment group). **(g)** qRT-PCR panel showing relative mRNA levels of Ca^{2+} channel-related genes (*CASQ2*, *ATP2A2*, *CACNA1C, RYR2,* and *SLC8A1),* K^+ channel-related genes (*KCNJ2*, *KCNA4*, *HCN1*, and *HCN4)* and Na^+ transporter-related gene *SCN5A* in hiPSC-CMs treated with EtOH for 5 weeks (n =3 cultures). Relative mRNA levels were calculated based on the average values of EtOH-treated group vs. untreated group. Comparisons were conducted between each treatment group and non-treatment group via two-sided Chi-square test for **(b)** and **(d)** or one-way ANOVA test for others. *, *P* value <0.05; **, *P* value <0.01; ***, *P* value <0.001; ****, *P* value <0.0001.

Fig. 5 Chronic EtOH treatment impairs contractility in hiPSC-CMs. **(a)** Representative traces showing the beating velocity recording of hiPSC-CMs treated with EtOH for 5 weeks. Blue dots indicate contraction, and red triangles indicate relaxation. **(b)** Quantification of maximum contraction velocity, maximum relaxation velocity, and beating rate changes (n =24 tissue sheets). **(c)** qRT-PCR panel showing relative mRNA levels of CM structure related genes in hiPSC-CMs treated with EtOH for 5 weeks (n =3 cultures).

Relative mRNA levels were calculated based on the average values of EtOH-treated group vs. untreated group. Comparisons were conducted between each treatment group and non-treatment group via one-way ANOVA test. *, *P* value <0.05; ***, *P* value <0.001; ****, *P* value <0.0001.

Fig. 6 Chronic EtOH treatment suppresses cardiac structure development in hiPSC-CMs. **(a)** Illustrative images presenting different levels of cardiac myofibrillar structure by α-actinin (green) and Hoechst (blue) staining. Score 1 cells are α-actinin-positive but without clear sarcomeric striations; Score 2 cells have diffused point staining pattern and striations in partial cell area; and Score 3 cells have organized, definitive myofibrillar structure with clear paralleled bands of z-discs distributed throughout the cell area. **(b)** Stacked bar chart showing proportions of hiPSC-CMs exhibiting each level of myofibrillar structure following the treatment with EtOH for 5 weeks. Sample sizes (n) were denoted at the top of each bar. **(c)** Quantification of α-actinin fluorescence intensity in hiPSC-CMs treated with EtOH for 5 weeks (n =5 cultures). **(d)** Quantification of cell spread area and circularity (cell width/ length) in hiPSC-CMs treated with EtOH for 5 weeks (n =75 cells for non-treatment group, 91 cells for 17 mM EtOH group, and 99 cells for 50 mM EtOH group). Relative MFI was calculated based on the average values of EtOH-treated group vs. untreated group. Comparisons were conducted between each treatment group and non-treatment group via two-sided Chi-square test for B or one-way ANOVA test for others. *, *P*-value <0.05; ***, *P*-value <0.001; ****, *P*-value <0.0001.

Fig. 7 Chronic EtOH treatment of hiPSC-CMs alters the expression of proteins identified by proteomic analysis. Proteomic analysis was performed to compare protein levels in hiPSC-CMs treated with EtOH for 5 weeks vs. non-treatment group. **(a)** Reproducibility of the biological duplicate experiments in each group. **(b)** Venn diagram showing the number of differentially expressed proteins in each treatment group. **(c)** Bar charts presenting top 15 upregulated and 5 downregulated GO terms based on *P* value and gene count enriched from DEPs in 17 or 50 mM EtOH-treated hiPSC-CMs. Length of bar indicates $-\log_{10}$(*P* value) and value of n denotes the count of proteins involved in each term. **(d)** Chord diagram showing connections

between the dysregulated proteins in 17 mM EtOH-treated hiPSC-CMs and the GO terms enriched from DEPs in both 17 and 50 mM EtOH treatment groups. GO terms were presented on the right and proteins contributing to these clusters were drawn on the left. The $\log_2$(fold change) for each protein is indicated with the red or blue color in the rectangles.

Figure 1

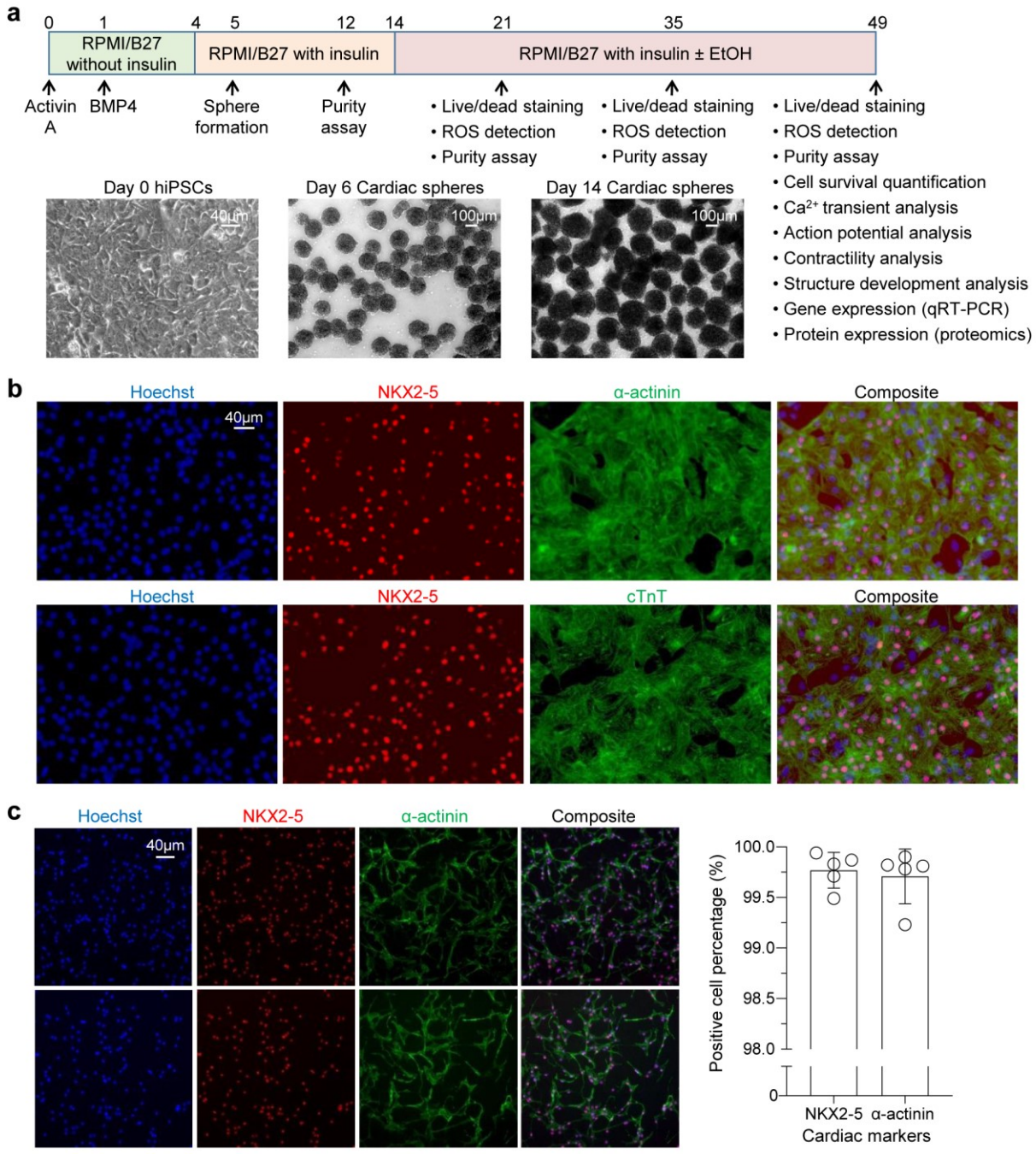
a
0
1
4
5
12
14
21
35
49
RPMI/B27 without insulin
RPMI/B27 with insulin
RPMI/B27 with insulin ± EtOH
Activin A
BMP4
Sphere formation
Purity assay
• Live/dead staining
• ROS detection
• Purity assay
• Live/dead staining
• ROS detection
• Purity assay
• Live/dead staining
• ROS detection
• Purity assay
• Cell survival quantification
• Ca2+ transient analysis
• Action potential analysis
• Contractility analysis
• Structure development analysis
• Gene expression (qRT-PCR)
• Protein expression (proteomics)
Day 0 hiPSCs
Day 6 Cardiac spheres
Day 14 Cardiac spheres
40μm
100μm
100μm
b
Hoechst
NKX2-5
α-actinin
Composite
40μm
Hoechst
NKX2-5
cTnT
Composite
c
Hoechst
NKX2-5
α-actinin
Composite
40μm
Positive cell percentage (%)
100.0
99.5
99.0
98.5
98.0
0
NKX2-5
α-actinin
Cardiac markers

Figure 2

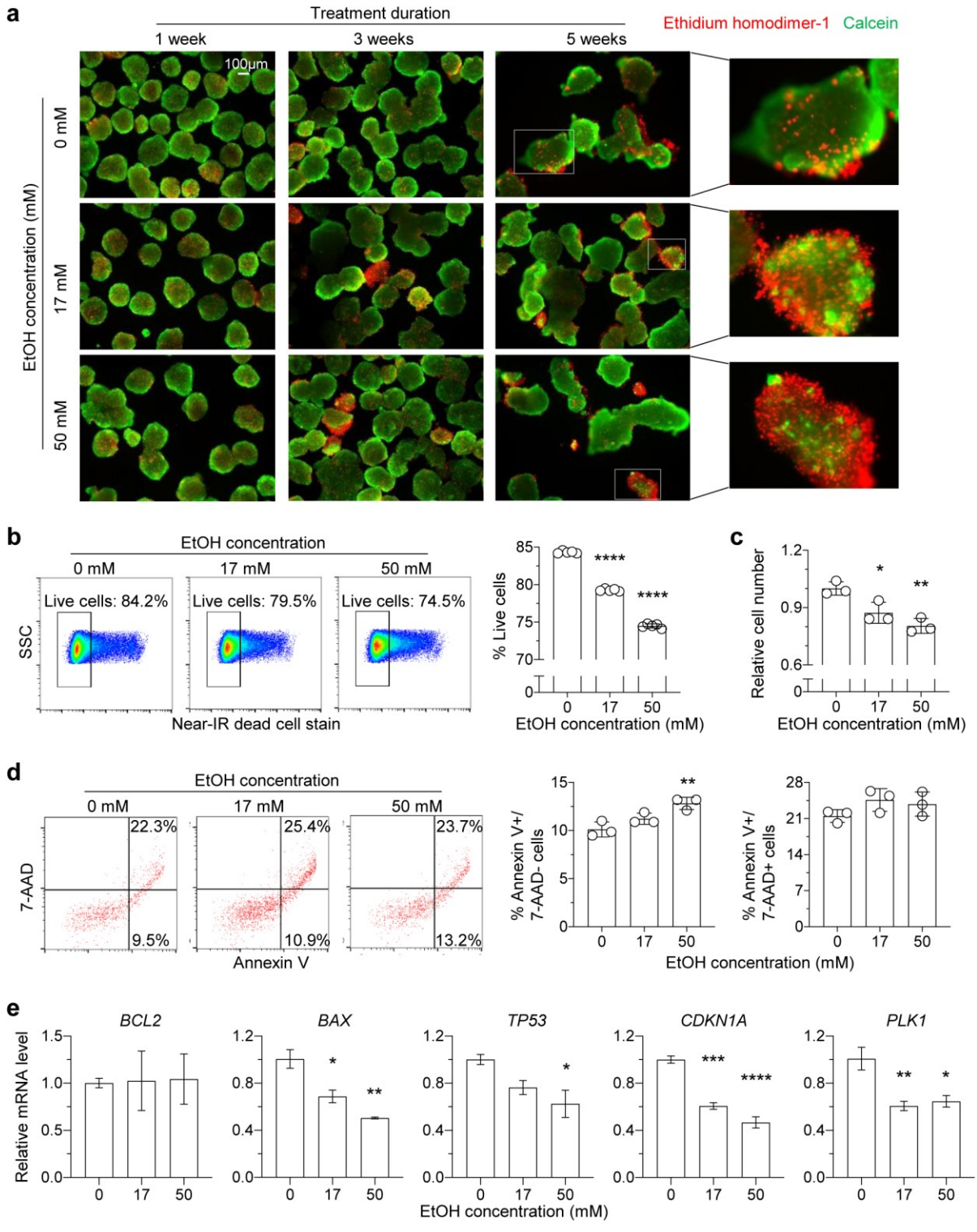
a
Treatment duration
1 week
3 weeks
5 weeks
Ethidium homodimer-1
Calcein
100μm
EtOH concentration (mM)
0 mM
17 mM
50 mM
b
EtOH concentration
0 mM
17 mM
50 mM
Live cells: 84.2%
Live cells: 79.5%
Live cells: 74.5%
SSC
Near-IR dead cell stain
% Live cells
****
****
EtOH concentration (mM)
c
Relative cell number
*
**
EtOH concentration (mM)
d
EtOH concentration
0 mM
17 mM
50 mM
22.3%
25.4%
23.7%
9.5%
10.9%
13.2%
7-AAD
Annexin V
% Annexin V+/ 7-AAD- cells
% Annexin V+/ 7-AAD+ cells
EtOH concentration (mM)
e
BCL2
BAX
TP53
CDKN1A
PLK1
Relative mRNA level
EtOH concentration (mM)

Figure 3

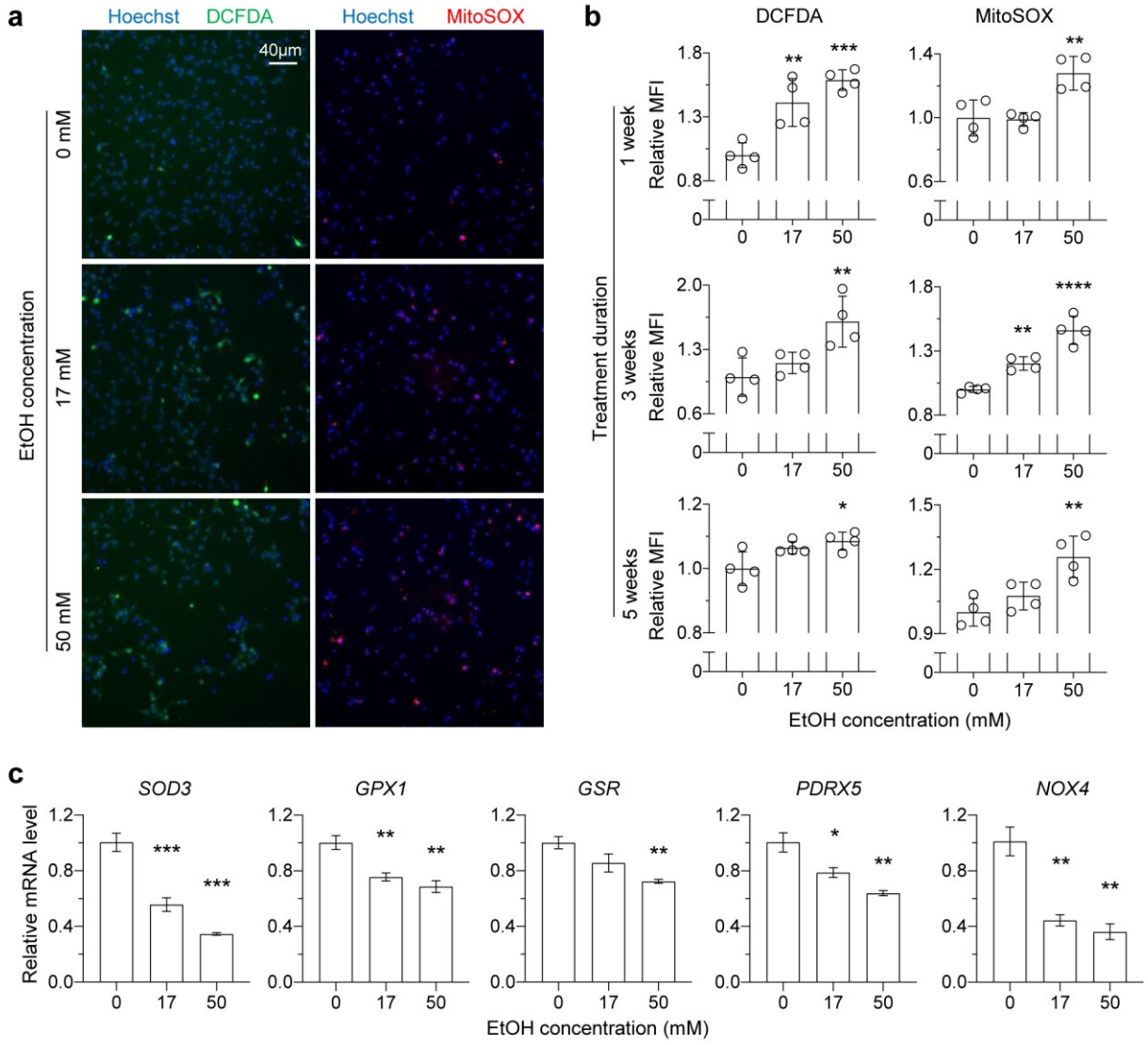
a
Hoechst
DCFDA
Hoechst
MitoSOX
40μm
EtOH concentration
0 mM
17 mM
50 mM
b
DCFDA
MitoSOX
Treatment duration
1 week
3 weeks
5 weeks
Relative MFI
EtOH concentration (mM)
c
SOD3
GPX1
GSR
PDRX5
NOX4
Relative mRNA level
EtOH concentration (mM)

Figure 4

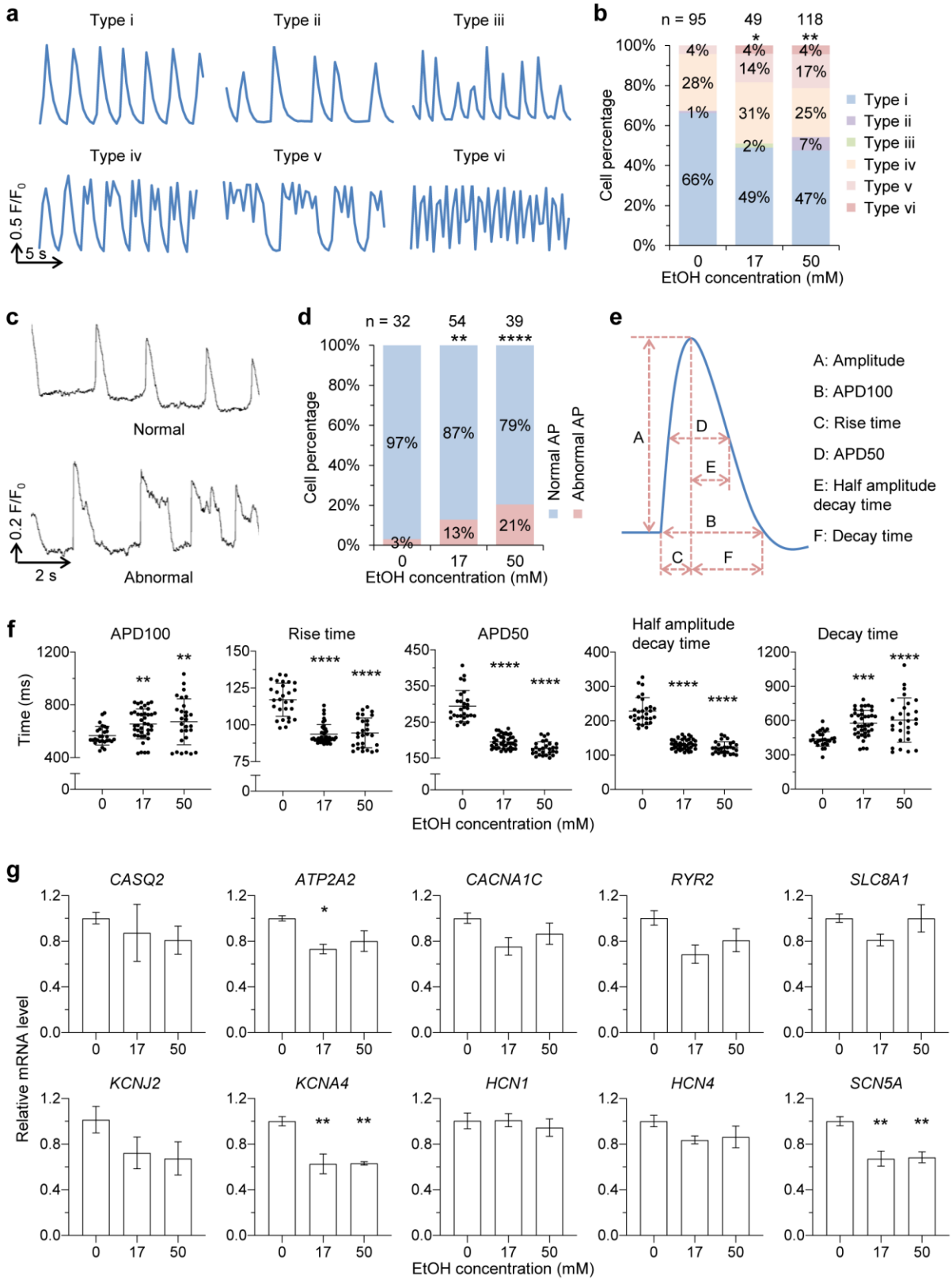
a
Type i
Type ii
Type iii
Type iv
Type v
Type vi
0.5 F/F0
5 s
b
n = 95
49
118
*
**
100%
80%
60%
40%
20%
0%
Cell percentage
4%
28%
1%
66%
4%
14%
31%
2%
49%
4%
17%
25%
7%
47%
Type i
Type ii
Type iii
Type iv
Type v
Type vi
0
17
50
EtOH concentration (mM)
c
Normal
0.2 F/F0
2 s
Abnormal
d
n = 32
54
39
**
****
100%
80%
60%
40%
20%
0%
Cell percentage
97%
3%
87%
13%
79%
21%
Normal AP
Abnormal AP
0
17
50
EtOH concentration (mM)
e
A
B
C
D
E
F
A: Amplitude
B: APD100
C: Rise time
D: APD50
E: Half amplitude decay time
F: Decay time
f
APD100
Rise time
APD50
Half amplitude decay time
Decay time
Time (ms)
1200
800
400
0
150
125
100
75
450
350
250
150
400
300
200
100
900
600
300
**
****
***
0
17
50
EtOH concentration (mM)
g
CASQ2
ATP2A2
CACNA1C
RYR2
SLC8A1
KCNJ2
KCNA4
HCN1
HCN4
SCN5A
Relative mRNA level
1.2
0.8
0.4
0.0
*
**
0
17
50
EtOH concentration (mM)

Figure 5

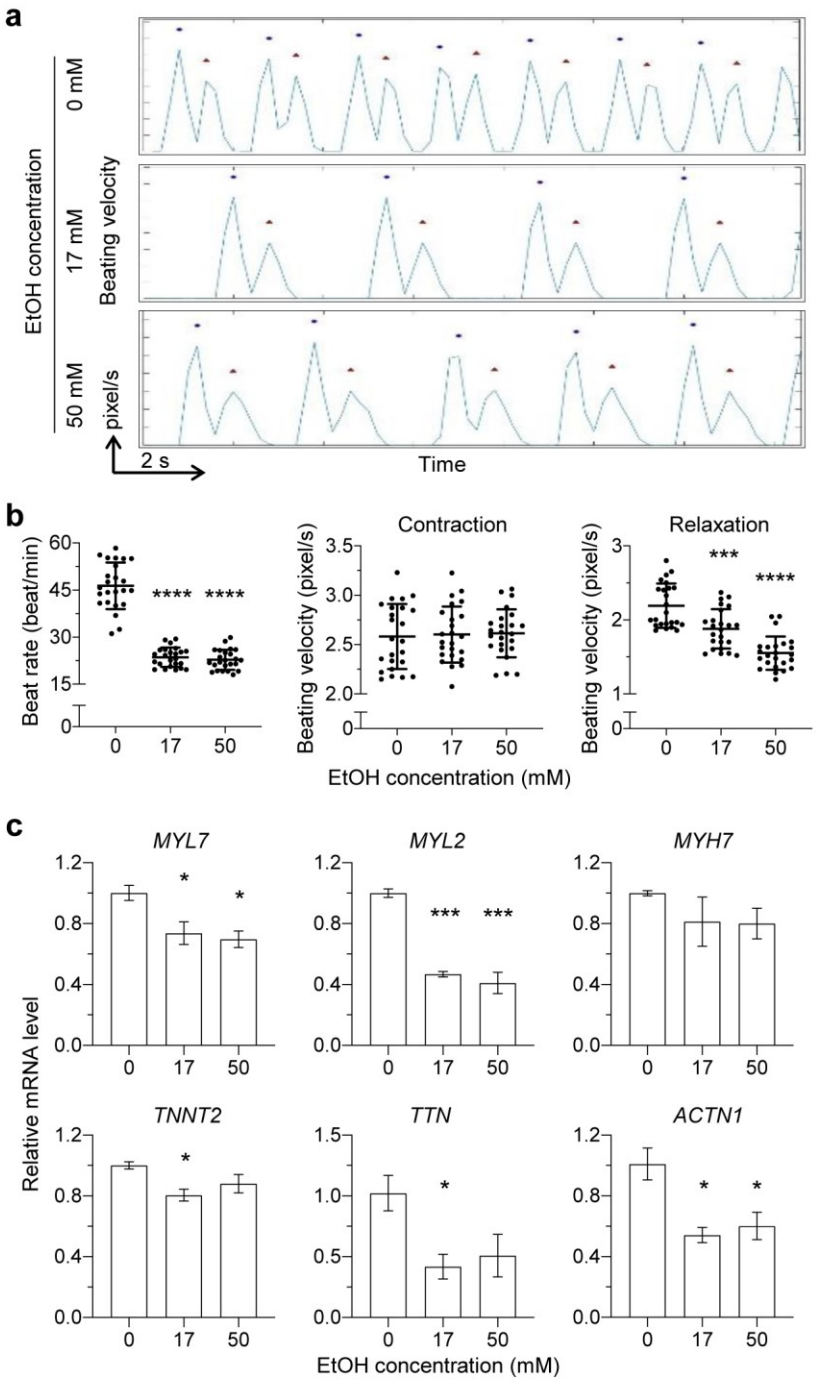
a
EtOH concentration
0 mM
17 mM
50 mM
Beating velocity
pixel/s
2 s
Time
b
Beat rate (beat/min)
Contraction
Relaxation
Beating velocity (pixel/s)
EtOH concentration (mM)
c
MYL7
MYL2
MYH7
TNNT2
TTN
ACTN1
Relative mRNA level
EtOH concentration (mM)

Figure 6

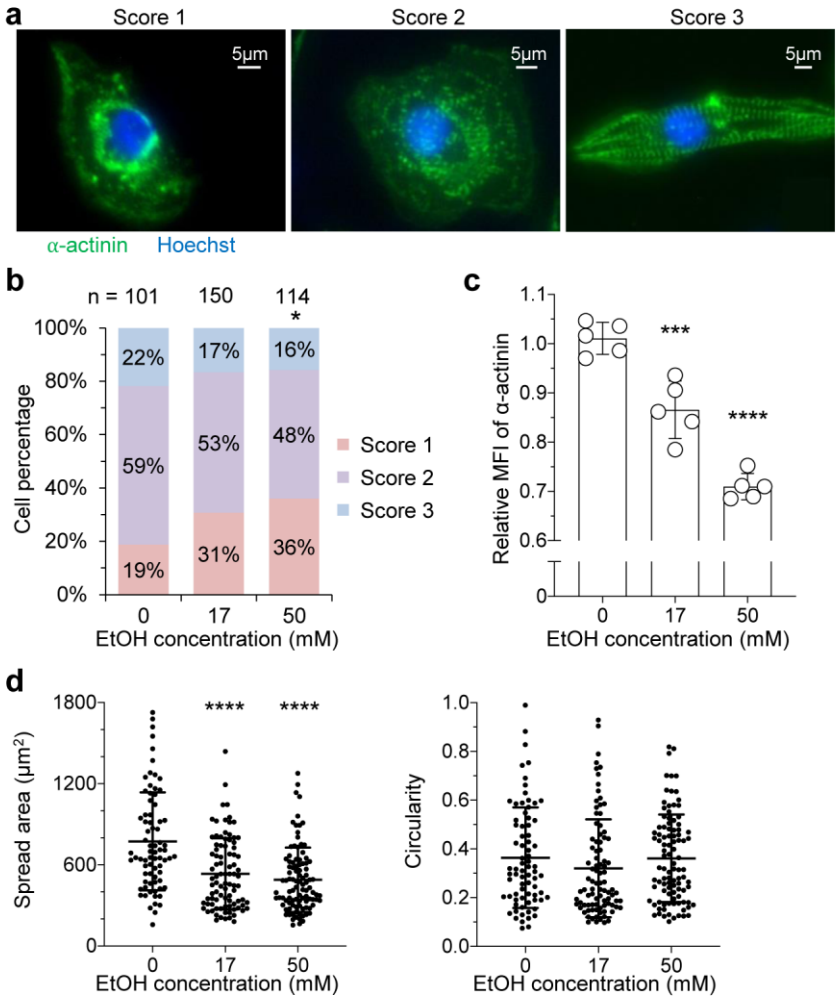
a
Score 1
Score 2
Score 3
5μm
α-actinin
Hoechst
b
n = 101
150
114
*
100%
80%
60%
40%
20%
0%
Cell percentage
22%
59%
19%
17%
53%
31%
16%
48%
36%
Score 1
Score 2
Score 3
0
17
50
EtOH concentration (mM)
c
Relative MFI of α-actinin
1.1
1.0
0.9
0.8
0.7
0.6
0
***
****
0
17
50
EtOH concentration (mM)
d
Spread area (μm²)
1800
1200
600
0
****
****
0
17
50
EtOH concentration (mM)
Circularity
1.0
0.8
0.6
0.4
0.2
0.0
0
17
50
EtOH concentration (mM)

Figure 7

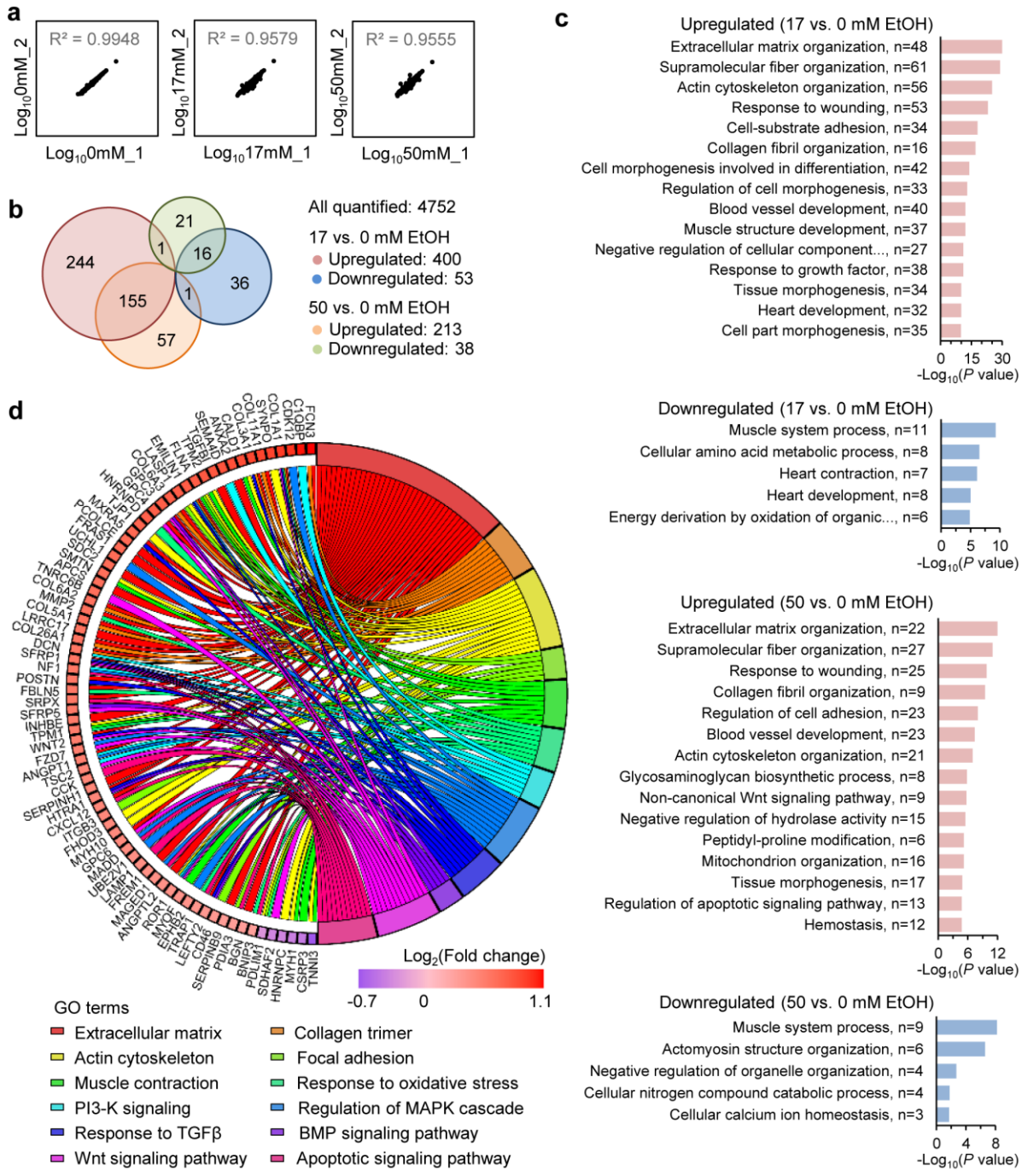
a
R² = 0.9948
R² = 0.9579
R² = 0.9555
Log10 0mM_2
Log10 17mM_2
Log10 50mM_2
Log10 0mM_1
Log10 17mM_1
Log10 50mM_1
b
244
21
1
16
36
155
1
57
All quantified: 4752
17 vs. 0 mM EtOH
Upregulated: 400
Downregulated: 53
50 vs. 0 mM EtOH
Upregulated: 213
Downregulated: 38
c
Upregulated (17 vs. 0 mM EtOH)
Extracellular matrix organization, n=48
Supramolecular fiber organization, n=61
Actin cytoskeleton organization, n=56
Response to wounding, n=53
Cell-substrate adhesion, n=34
Collagen fibril organization, n=16
Cell morphogenesis involved in differentiation, n=42
Regulation of cell morphogenesis, n=33
Blood vessel development, n=40
Muscle structure development, n=37
Negative regulation of cellular component..., n=27
Response to growth factor, n=38
Tissue morphogenesis, n=34
Heart development, n=32
Cell part morphogenesis, n=35
0 15 30
-Log10(P value)
Downregulated (17 vs. 0 mM EtOH)
Muscle system process, n=11
Cellular amino acid metabolic process, n=8
Heart contraction, n=7
Heart development, n=8
Energy derivation by oxidation of organic..., n=6
0 5 10
-Log10(P value)
Upregulated (50 vs. 0 mM EtOH)
Extracellular matrix organization, n=22
Supramolecular fiber organization, n=27
Response to wounding, n=25
Collagen fibril organization, n=9
Regulation of cell adhesion, n=23
Blood vessel development, n=23
Actin cytoskeleton organization, n=21
Glycosaminoglycan biosynthetic process, n=8
Non-canonical Wnt signaling pathway, n=9
Negative regulation of hydrolase activity n=15
Peptidyl-proline modification, n=6
Mitochondrion organization, n=16
Tissue morphogenesis, n=17
Regulation of apoptotic signaling pathway, n=13
Hemostasis, n=12
0 6 12
-Log10(P value)
Downregulated (50 vs. 0 mM EtOH)
Muscle system process, n=9
Actomyosin structure organization, n=6
Negative regulation of organelle organization, n=4
Cellular nitrogen compound catabolic process, n=4
Cellular calcium ion homeostasis, n=3
0 4 8
-Log10(P value)
d
Log2(Fold change)
-0.7 0 1.1
GO terms
Extracellular matrix
Actin cytoskeleton
Muscle contraction
PI3-K signaling
Response to TGFβ
Wnt signaling pathway
Collagen trimer
Focal adhesion
Response to oxidative stress
Regulation of MAPK cascade
BMP signaling pathway
Apoptotic signaling pathway

Supplementary Information

Chronic ethanol exposure induces deleterious changes in cardiomyocytes derived from human induced pluripotent stem cells

Rui Liu, Fangxu Sun, Lawrence C. Armand, Ronghu Wu, and Chunhui Xu

Table S1. Information of major reagents

Product Name	Supplier	Catalog#
mTeSR1 defined medium	Stem Cell Technologies	85850
RPMI 1640 medium	Thermo Fisher Scientific	11875093
B27 Supplement (50X), minus insulin	Thermo Fisher Scientific	A1895601
B27 Supplement (50X), serum free	Thermo Fisher Scientific	17504044
Pen Strep	Gibco	15140-122
Matrigel	Thermo Fisher Scientific	CB40230C
Activin-A Protein	R&D Systems	338-AC-050/CF
BMP-4 Protein	R&D Systems	314-BP/CF
DMEM (1X)	Gibco	11995-065
0.25% Trypsin-EDTA (1X)	Fisher Scientific	25200-114
Fetal Bovine Serum Characterized	HyClone	SH30396.03
Rock Inhibitor (Y-276322HCl)	Selleckchem	S1049
AggreWell400, 24-well plate	Stem Cell Technologies	34415
Paraformaldehyde	Electron Microscopy Sciences	15710
BSA Solution, 30%	MilliporeSigma	A9576
Hoechst33342	Thermo Fisher Scientific	H3570
Ethyl Alcohol	MilliporeSigma	E7023
Mineral oil	MilliporeSigma	M5310
Dimethyl sulfoxide	MilliporeSigma	D2438
Live/Dead Viability/Cytotoxicity Kit	Invitrogen	L3224
Live/Dead Fixable Near-IR Dead Cell Stain Kit	Thermo Fisher Scientific	L34976
PE Annexin V Apoptosis Detection Kit	BD Biosciences	559763
Fluo-4, AM	Thermo Fisher Scientific	F14201
FluoVolt	Thermo Fisher Scientific	F10488
Image-iT LIVE Green Reactive Oxygen Species Detection Kit (DCFDA)	Thermo Fisher Scientific	I36007
MitoSOX Red Mitochondrial Superoxide Indicator	Thermo Fisher Scientific	M36008
Aurum Total RNA Mini Kit	Bio-Rad	732-6820
SuperScript VILO cDNA Synthesis Kit	Thermo Fisher Scientific	11754050
iTaq SyBr Green Master Mix	Bio-Rad	172-5121
GeneMate 96-Well PCR Plates (Semi-Skirted)	VWR	490003-822

Table S2. Antibodies for immunocytochemistry

Type	Target	Isotype	Supplier	Catalog#	Dilution
Primary	α-actinin	mouse IgG_1	Sigma	A7811	1:800
	NKX2-5	rabbit IgG	Cell Signaling Technologies	8792S	1:800
	cardiac troponin T	mouse IgG_1	Fisher Scientific	MS295P1	1:200
Secondary	Alexa 488, Goat anti-mouse IgG1		Invitrogen	A-21121	1:1000
	Alexa 594, Goat anti-rabbit IgG		Invitrogen	A-11012	1:1000

Table S3. Primers for qRT-PCR

Gene	Full name	Accession code	Primer sequence
BCL2	B-cell CLL/lymphoma 2	NM_000633.2	Forward: GAGAAATCAAACAGAGGCCG Reverse: CTGAGTACCTGAACCGGCA
BAX	BCL2-associated X	NM_004324	Forward: GGAGGAAGTCCAATGTCCAG Reverse: TCTGACGGCAACTTCAACTG
TP53	Tumor protein P53	NM_000546	Forward: CAGCACATGACGGAGGTTGT Reverse: TCATCCAAATACTCCACACGC
CDKN1A	Cyclin-dependent kinase inhibitor 1A	NM_000389	Forward: CATGGGTTCTGACGGACAT Reverse: AGTCAGTTCCTTGTGGAGCC
CDKN1B	Cyclin-dependent kinase inhibitor 1B	NM_004064	Forward: AACGTGCGAGTGTCTAACGG Reverse: CCCTCTAGGGGTTTGTGATTCT
PLK1	Polo-like kinase 1	NM_005030	Forward: AGTCGACCACCTCACCTGTC Reverse: GCCCCTCACAGTCCTCAATA
SOD1	Superoxide dismutase 1	NM_000454	Forward: GGTGGGCCAAAGGATGAAGAG Reverse: CCACAAGCCAAACGACTTCC
SOD2	Superoxide dismutase 2	NM_000636	Forward: GCTCCGGTTTTGGGGTATCTG

			Reverse: GCGTTGATGTGAGGTTCCAG
SOD3	Superoxide dismutase 3	NM_003102	Forward: ATGCTGGCGCTACTGTGTTC Reverse: CTCCGCCGAGTCAGAGTTG
GSR	Glutathione reductase	NM_001195102	Forward: CACTTGCGTGAATGTTGGATG Reverse: TGGGATCACTCGTGAAGGCT
GPX1	Glutathione peroxidase 1	NM_201397	Forward: CAGTCGGTGTATGCCTTCTCG Reverse: GAGGGACGCCACATTCTCG
NQO2	NAD(P)H dehydrogenase, quinone 2	NM_000904	Forward: GTACTCATTGTCTATGCACACCA Reverse: TGCCTGCTCAGTTCATCTACA
PRDX5	Peroxiredoxin 5	NM_181651	Forward: TCCTGGCTGATCCCACTGG Reverse: CTGTGAGATGATATTGGGTGCC
NOX1	NADPH oxidase 1	NM_007052	Forward: CTGCTTCCTGTGTGTCGCAA Reverse: AGGCAGATCATATAGGCCACC
NOX4	NADPH oxidase 4	NM_001143836	Forward: CAGATGTTGGGGCTAGGATTG Reverse: GAGTGTTCGGCACATGGGTA
NOX5	NADPH oxidase 5	NM_001184780	Forward: CTATTGGACTCACCTGTCCTACC

			Reverse: GGAAAAACAAGATTCCAGGCAC
DUOX1	Dual oxidase 1	NM_017434	Forward: GCAGCGATTTGATGGGTGGTA Reverse: AGGTGGGGTTCTCCCAAGG
DUOX2	Dual oxidase 2	NM_014080	Forward: ACGGTGTGTATCAGGCTCTG Reverse: CACGTCGGAAAGAACATGGTAG
RYR2	Ryanodine receptor 2	NM_001035	Forward: CAAATCCTTCTGCTGCCAAG Reverse: CGAAGACGAGATCCAGTTCC
CACNA1C	Calcium voltage-gated channel subunit alpha 1C	NM_000719	Forward: TTTTAAAAACGCTTCCACCG Reverse: TTCCAGAAGATGATTCCAACG
ATP2A2	ATPase sarcoplasmic/endoplasmic reticulum Ca^{2+} transporting 2	NM_170665	Forward: TCAGCAGGAACTTTGTCACC Reverse: GGGCAAAGTGTATCGACAGG
CASQ2	Calsequestrin 2	NM_001232	Forward: TTATGTTCAAGGACCTGGGC Reverse: GCCTCTACTACCATGAGCCG
SLC8A1	Solute carrier family 8, member A1	NM_021097	Forward: CTGGAATTCGAGCTCTCCAC Reverse: ACATCTGGAGCTCGAGGAAA
KCNJ2	Potassium inwardly rectifying channel subfamily J member 2	NM_000891	Forward: TGACTCAGCTGACATCCAGA

			Reverse: TTACATGCCTCTGTACCCCC
KCNA4	Potassium voltage-gated channel subfamily A member 4	NM_002233	Forward: CAGAGCATTCTTCAGCCAAA Reverse: CAGCCGGTGGATTTTCTTTA
HCN1	Hyperpolarization activated cyclic nucleotide-gated potassium channel 1	NM_021072	Forward: ACTGCACTGGCGAGATCATA Reverse: CAAAAATTCTCAGTCTCTTGCGT
HCN4	Hyperpolarization activated cyclic nucleotide-gated potassium channel 4	NM_005477	Forward: GACCCGCAGCGGATTAAAATG Reverse: ATGCGTGTCTCCACAATGAGG
SCN5A	Sodium voltage-gated channel alpha subunit 5	NM_000335	Forward: TGCTGTGAAAATCCCTGTGA Reverse: TCAACACACTCTTCATGGCG
TNNT2	Troponin T type 2	NM_001001431	Forward: GCGGGTCTTGGAGACTTTCT Reverse: TTCGACCTGCAGGAGAAGTT
TTN	Titin	NM_133378	Forward: GGGTTCGATTTTCCTCTTGA Reverse: AGCCAACCTGAGTCTGGAAG
ACTN1	Actinin alpha 1	NM_001102	Forward: AGGTGGGAGTTACACCATGC Reverse: ACATGCAGCCAGAAGAGGAC
MYH6	Myosin heavy chain 6	NM_002471	Forward: CTTCTCCACCTTAGCCCTGG

			Reverse: GCTGGCCCTTCAACTACAGA
MYH7	Myosin heavy chain 7	NM_000257	Forward: CGCACCTTCTTCTCTTGCTC Reverse: GAGGACAAGGTCAACACCCT
MYL2	Myosin light chain 2	NM_000432	Forward: CGTTCTTGTCAATGAAGCCA Reverse: CAACGTGTTCTCCATGTTCG
MYL7	Myosin light chain 7	NM_021223	Forward: CTTGTAGTCGATGTTCCCCG Reverse: TCAAGCAGCTTCTCCTGACC
GAPDH	Glyceraldehyde-3-phosphate dehydrogenase	NM_001256799	Forward: CTGGGCTACACTGAGCACC Reverse: AAGTGGTCGTTGAGGGCAATG

Table S4. Top 15 up- and downregulated proteins in hiPSC-CMs upon 17 and 50 mM EtOH treatment for 5 weeks identified by proteomics.

Upregulated				Downregulated			
Symbol	Fold change (17 vs. 0)	Symbol	Fold change (50 vs. 0)	Symbol	Fold change (17 vs. 0)	Symbol	Fold change (50 vs. 0)
ATP13A3	2.590	IGFN1	7.013	TNNI3	0.629	TNNI3	0.697
MOB3C	2.285	CCK	5.975	NACA	0.703	CRYAB	0.714
SARM1	2.278	MOB3C	2.878	CSRP3	0.735	SLMAP	0.715
COX14	2.246	CCDC51	2.635	MYH1	0.752	ACTA1	0.719
FCN3	2.143	ATP13A3	2.338	TSC22D2	0.767	CSRP3	0.727
C1QBP	2.107	CDK12	2.318	CKM	0.768	HNRNPC	0.743
CMBL	2.021	COX14	2.296	HNRNPC	0.771	CASQ1	0.747
CDK12	1.973	CMBL	2.234	SDHAF2	0.774	ADPRHL1	0.748
COL1A1	1.925	PLCB4	2.172	NACA	0.778	MAP4	0.756
EPN1	1.923	C1QBP	2.083	IMPA1	0.790	CKM	0.761
RTCA	1.903	ATP5J	2.027	WDR46	0.801	SNRPE	0.769
SYNPO	1.877	EPN1	1.960	MAP4	0.802	SSB	0.770
COL11A1	1.871	HNRNPD	1.952	REXO1L2P	0.810	PCIF1	0.779
COL3A1	1.853	FNBP1L	1.861	ADPRHL1	0.811	REXO1L2P	0.789
UBFD1	1.853	GAS2L3	1.839	SSB	0.818	TAGLN2	0.795

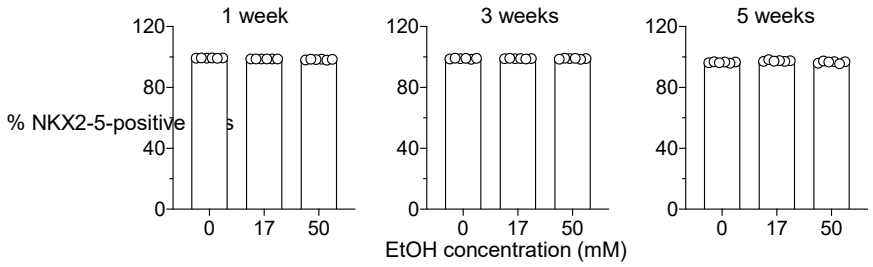

Fig. S1 Chronic EtOH exposure has no impact on hiPSC-CM purity. Quantification of NKX2-5-positive cells in hiPSC-CMs treated with EtOH for 1, 3, and 5 weeks (n = 6 cultures). Comparisons were conducted between each treatment group and no treatment group via One-way ANOVA test.

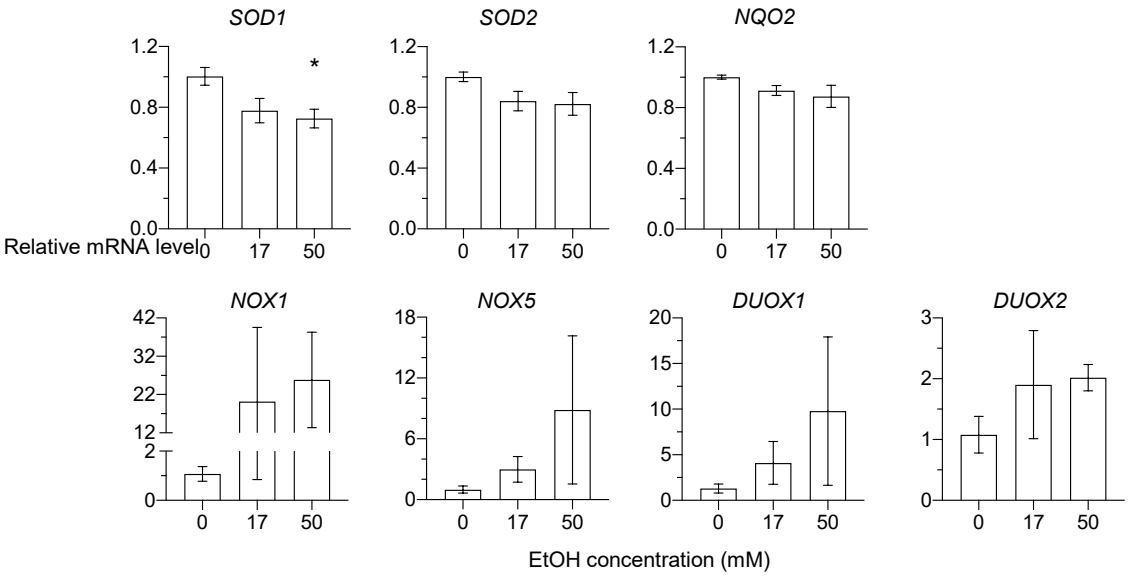

Fig. S2 Chronic EtOH treatment causes oxidative stress in hiPSC-CMs. qRT-PCR analysis showing relative mRNA levels of oxidative stress-related genes in hiPSC-CMs treated with EtOH for 5 weeks (n = 3 cultures). Relative mRNA levels were calculated based on the average values of EtOH-treated group vs. untreated group. Comparisons were conducted between each treatment group and no EtOH group via One-way ANOVA test. *, *P*-value < 0.05.

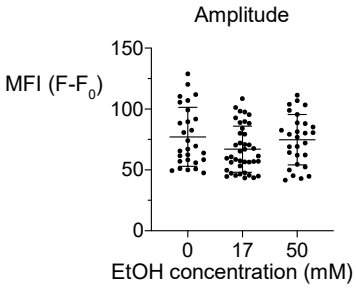

Fig. S3 Chronic EtOH treatment damages AP in hiPSC-CMs. Quantification of AP amplitude in hiPSC-CMs following the treatment with EtOH for 5 weeks (n = 28 cells for 0 and 50 mM EtOH treatment groups, n = 40 cells for 17 mM EtOH treatment group). Comparisons were conducted between each treatment group and no treatment group via One-way ANOVA.

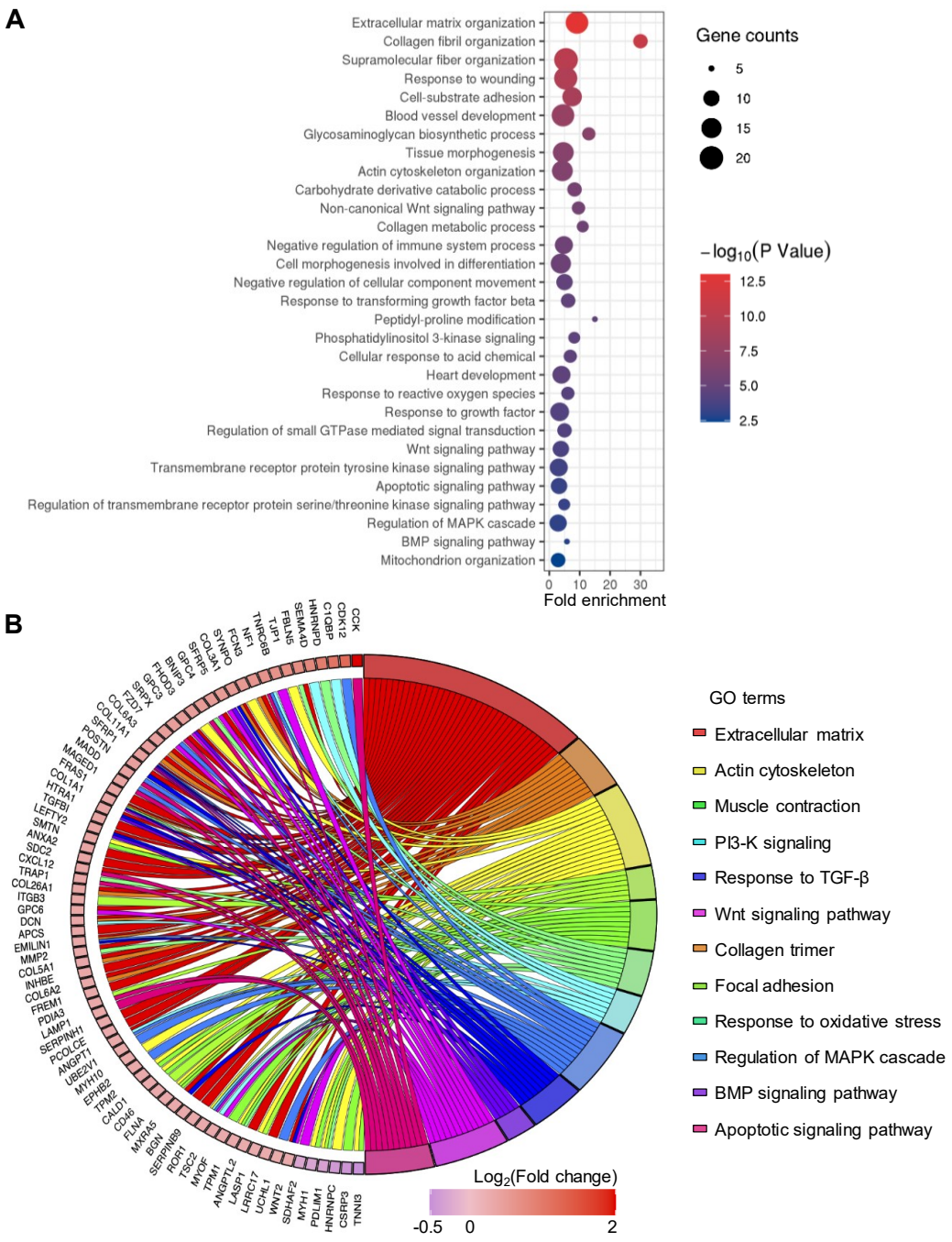

Fig. S4 Chronic EtOH treatment of hiPSC-CMs alters the expression of proteins identified by proteomic analysis. Proteomic analysis of hiPSC-CMs treated with EtOH for 5 weeks. **(a)** Bubble plot presenting top 30 upregulated GO terms based on *P* value and gene count enriched from DEPs in both 17 and 50 mM EtOH treated hiPSC-CMs. The red or blue color of bubbles indicates $-\log_{10}(P \text{ value})$ and the area indicates the number of involved proteins in each GO term. **(b)** Chord diagram showing connections between the dysregulated proteins in 50 mM EtOH treated hiPSC-CMs and the interested GO terms enriched from DEPs in both 17 and 50 mM EtOH treatment groups. GO terms were presented on the right and proteins contributing to these clusters were drawn on the left. The $\log_2$(fold change) for each protein is indicated with the red or blue color in the rectangles.